DANILO HENRIQUE COSTA SOUZA

ROBOTIC ARM USING STEP MOTORS: STUDIES FOR OPTIMAL OPERATION AND LOAD MASS ESTIMATION

São Paulo
2021

DANILO HENRIQUE COSTA SOUZA

ROBOTIC ARM USING STEP MOTORS: STUDIES FOR OPTIMAL OPERATION AND LOAD MASS ESTIMATION

Dissertation submitted to Escola Politécnica of the Universidade de São Paulo for degree of Master in Science.

São Paulo
2021

DANILO HENRIQUE COSTA SOUZA

ROBOTIC ARM USING STEP MOTORS: STUDIES FOR OPTIMAL OPERATION AND LOAD MASS ESTIMATION

Revised Version

Dissertation submitted to Escola Politécnica of the Universidade de São Paulo for degree of Master in Science.

Concentration area:

Systems engineering

Advisor:

Prof. Dr. Diego Colón

São Paulo
2021

Este exemplar foi revisado e corrigido em relação à versão original, sob responsabilidade única do autor e com a anuência de seu orientador.

São Paulo, 03 de Fevereiro de 2021

Assinatura do autor: Danilo H. C. Souza

Assinatura do orientador: Diego Colón

Catalogação-na-publicação

Souza, Danilo Henrique
Robotic arm using step motors: studies for optimal operation and load mass estimation / D. H. Souza -- versão corr. -- São Paulo, 2021.
84 p.

Dissertação (Mestrado) - Escola Politécnica da Universidade de São Paulo. Departamento de Engenharia de Telecomunicações e Controle.

1.Step motor 2.Step driver 3.Dynamic load 4.Performance analysis 5.Load mass estimation I.Universidade de São Paulo. Escola Politécnica. Departamento de Engenharia de Telecomunicações e Controle II.t.

ACKNOWLEDGMENTS

To my wife for the support during the study times and the understanding during the absence times.

To my teacher and advisor Diego Colón for the countless hours of guidance through this work and for embracing the idea.

"Love is the one thing that transcends time and space."

-Interstellar, 2014.-

RESUMO

Motores de passo podem ser descritos como motores DC digitais onde é possível obter um movimento preciso e bem definido. Entretanto, são sistemas não-lineares bastante complexos os quais precisam de um *driver* específico para realizar a interface entre o motor e o controlador digital a fim de obter o desempenho desejado. Os componentes supracitados formam um *Step System* e são a forma mais comum de utilização de motores de passo. O *driver*, incluído nas análises e simulações realizadas, proporciona um cenário mais próximo de uma sistema prático. Este trabalho combina as equações elétricas e mecânicas do modelo do motor de passo com as equações dinâmicas de um braço robótico de um grau de liberdade, com o intuito analisar o desempenho do sistema por meio de um *framework*, a análise proposta é realizada via *Simulink*© e inclui a modelagem completa do driver, consistindo em analisar o tempo, o passo médio do motor e a eficiência energética do sistema completo. O Objetivo final é propor um método para estimação da massa da carga quando o motor está parado com corrente fluindo nas bobinas.

Palavras-Chave: Motor de passo, micro passo, carga dinâmica, análise de desempenho, *chopper driver*.

ABSTRACT

Step motors can be described as digital DC motors where it is possible to obtain a very precise and fixed motion. They are, however, a rather complex non linear systems that need a specific driver for interfacing with a digital controller in order to achieve the desired performance. The aforementioned components compose a so called *Step System* and are the most common way of operating a step motor. The step driver, included in the simulations and analysis here performed, makes the scenario more close to a practical one. This work combines the step motor electrical and mechanical equations, with the dynamics of a 1 DOF robotic arm to analyse the performance of the system through a performance analysis framework, performed via *Simulink*© including the model of the driver, which consists of analysing the time, the mean of the actual stepped angle of the motor and energy efficiency and consumption of the whole system. The final goal is to propose a method to estimate the mass of the load when the motor is stopped with current flowing through its windings.

Keywords: Step motor, micro stepping, step driver, dynamic load, performance analysis, chopper driver.

LIST OF FIGURES

LIST OF TABLES

LIST OF SYMBOLS

θ_1	Angle of the arm with respect to the horizontal axis
θ_m	Angle of the motor's axis with respect to the horizontal axis
$\dot{\theta_1}$	Arm's speed
$\ddot{\theta_1}(t)$	Acceleration of the arm
τ_l	Load torque
$i_j(t)$	Current on the *j-th* phase of the step motor
m_g	Mass of the grip
τ_L	Load torque
$\mathbf{v}$	Velocity vector of the load
$\delta\theta$	Step angle of the step motor
τ_f	Torque needed to move the load
τ_m	Torque of the motor
N_p	Total number of pulses to move the motor through a given distance
t_{sim}	Power step motor module simulation time in $Simulink^{©}$
PPS_{ref}	Driver reference frequency given in pulses per second

LIST OF ACRONYMS

c.g	Center of Gravity
D.O.F.	Degree of Freedom
RMS	Root Mean Square
IC	Integrated Circuit
CNC	Computer Numeric Control
PWM	Pulse Width Modulation
RPM	Rotations Per Minute
PM	Permanent Magnet
MOSFET	Metal-Oxide-Semiconductor Field Effect Transistor
PCB	Printed Circuit Board
VDC	Voltage DC
PLC	Programmable Logic Controller
EMF	Electromotive force
PPR	Pulses Per Revolution
PPS	Pulses Per Second
AI	Artificial Intelligence

CONTENTS

1 INTRODUCTION

This chapter presents an introduction of the problem to be analysed as well as a literature review on the matter and the structure of this work.

1.1 The motivating problem

The problem behind this work comes from a machine developed for paring the coconut's skin, as one of the last steps in coconut processing. The machine must process a half of a coconut at a time. The coconut half is placed on a table and transported by a one degree of freedom robotic arm, known as the feeder arm, to the next step, which is the paring table, that will do the actual work of removing the coconut's skin. Figure 1 shows a coconut and it's layers.

Figure 1: Layers of a coconut.

Source: *The author*

The feeder arm is driven by a NEMA 34 step motor powered by an external $6A$ step driver. This driver was built specifically for this application using an external MOSFET's driver and a microcontroller for interfacing. The need to built a specially designed driver comes from the fact that the arm is heavy and even though a gear-box is used to counter-balance the hight torque needed, this leads to the most common problem when it comes to step motors: *the Speed X Torque* curve, that is, using high torque in a high speed application implies step loss, hence the need to perform a careful selection.

Most of step motor papers do not clearly indicate, or do not use, a model for the load torque and usually simulates the equations of the motor using a step input voltage. This work intends to combine both step motor's electrical and mechanical models with the dynamic model of a 1 D.O.F robotic arm to study its behaviour when transporting a non static load through long distances, usually higher than 10 times the base step $\delta\theta = 1.8^{\circ}$. Energizing a step motor is a far complex task and it is usually done by an external driver. This work analyses the behaviour of a step motor when energized by a step driver. The driver controls the current on the motor's windings via PWM voltage (detailed in Section 2.3).

Also, it is desired to control the arm's displacement from one given position to another in minimum time. The arm is not supposed to move at a target speed, but it is required to move a fixed distance in minimum time. The frequency in which the chosen step motor will begin to not respond to command pulses gives the upper boundary speed for the system and, therefore, is the time limiting factor of the problem. Before presenting the operation of the arm, it is important to properly reference the reader for the angles variables used in this work. In the reference chosen, the load angle θ_L is equal to the motor's angle θ_m (detailed in section 3.1), which may also be referred to as θ_1.

The total displacement required for the arm to move varies and there are four states (positions) that the arm can be stationary while waiting to move again. They are:

1. **Wait Load:** Position where the arm waits the command to pick up the coconut ($\theta_L = 135^{\circ}$);
2. **Load:** Position where the arm picks up the coconut ($\theta_L = 180^{\circ}$);
3. **Wait Unload:** Position where the arm waits the command to place the coconut at the paring table ($\theta_L = 45^{\circ}$);
4. **Unload:** Position where the arm releases the coconut at the paring table ($\theta_L = 0^{\circ}$).

Figure 2 shows a full cycle, from picking up the coconut to place it at the paring table of the feeder arm operation.

This arrangement with the feeder arm to place the coconuts into the machine gives the possibility of adding a buffer to the whole process, that is, the arm is always picking up a coconut while the paring table is processing. This shortens the time to place the next coconut into the machine. However, the arm must be fast enough in order to have the buffer always full at the "Wait Load" position before the machine finishes an operation.

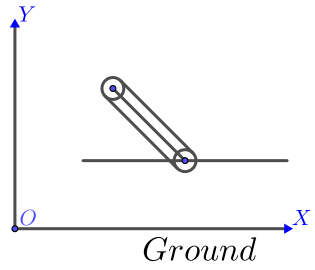

(a) Step 1: Wait Load: $\theta_m = 135^o$

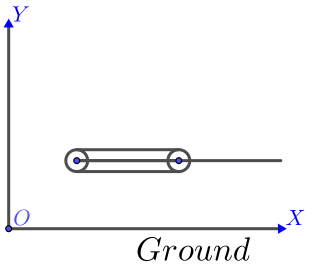

(b) Step 2: Load: $\theta_m = 180^o$

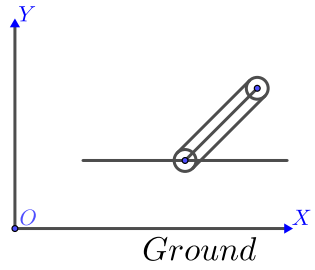

(c) Step 3: Wait Unload: $\theta_m = 45^o$

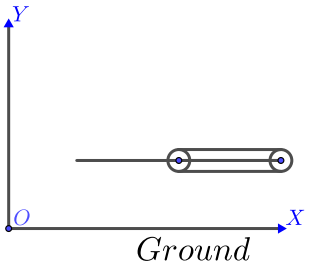

(d) Step 4: Unload: $\theta_m = 0^o$

Figure 2: Work positions of the arm.

Source: *The author*

There are a few scenarios where this arrangement is interrupted, for example, in a case where the coconut is rejected by the machine and the arm is still at the "Load" position. This would lead to a state where the arm would go straight from "Load" to "Unload", since the buffer is empty.

Some of the system's operating scenarios are described below:

- Normal operation
  - $1 \rightarrow 2$ Pick up the coconut: $\Delta\theta = 45^o$
  - $2 \rightarrow 3$ Wait to place the coconut: $\Delta\theta = 135^o$
  - $3 \rightarrow 4$ Place a coconut form the buffer into the machine: $\Delta\theta = 45^o$
  - $4 \rightarrow 1$ Wait to pick up the coconut: $\Delta\theta = 135^o$
- Alternative operation
  - $1 \rightarrow 2$ Pick up the coconut: $\Delta\theta = 45^o$
  - $2 \rightarrow 4$ Pick up the coconut at the buffer plate and place it into the paring table: $\Delta\theta = 180^o$
  - $4 \rightarrow 1$ Wait to pick up the coconut: $\Delta\theta = 135^o$

Ideally, the system displacements are multiples of 45^o degrees, but this is for representation purposes. In practice the "Unload" position can, and should, be configured for minimize the time to place the coconut into the paring table. Since this system is here modelled using both the load and the actuator models, a performance analysis framework is also proposed to enlighten and establish useful parameters to be analysed when working with step motors on the edge of their operation.

1.2 Step motors

Step motors have been widely studied since they first came to be in the early 1960's (KHAN; TAJ; IJAZ, 2014) and are mainly applied to motion problems due to a number of benefits: high precision (synchronous), simple control, can be used in open loop (with restrictions), low cost, low heat, reduced noise and low maintenance.

They are used in many applications nowadays such as 2D and 3D printers, disc head drivers and small positioning machines due to its capacity of precise positioning and ease of control. (HUGHES; DRURY, 2013).

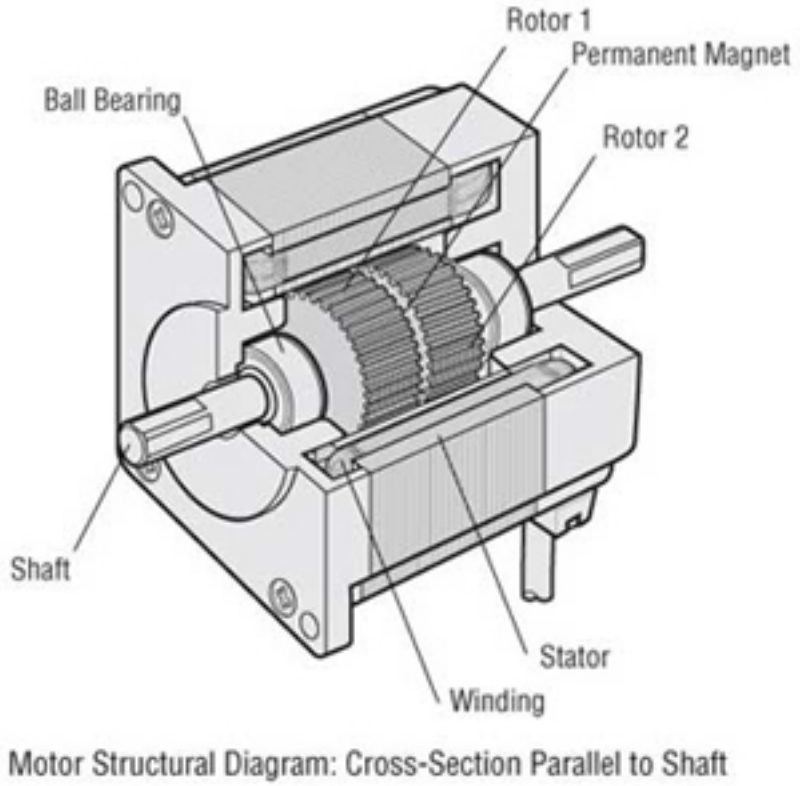

Figure 3: Cross section of a step motor.
Source: *https://www.orientalmotor.com.br/motores-de-passo/technology/stepper-motor-overview.html*

On the other hand, they present a very critical downside, which is the loss of torque as

speed increases (HUGHES; DRURY, 2013), so high speed applications that require high torque are not suitable for step motors. They are, still, a very interesting alternative to high cost servo systems in applications with low torque demand. The concept, however, of what can be considered high torque and low torque is relative and depends on a variety of aspects of the system design.

There are three types of step motors construction: Permanent Magnet (PM), Variable Reluctance (VR) and Hybrid, which is a combination of the previous two. The last being most widely used step motor nowadays due to its simplicity of operation when combined with the proper step driver. Figure 3 shows the cross section of a hybrid step motor. which is the motor used in this work. The motor itself is just a part of a *Step System*, shown in Figure 4, composed by the step motor, a driver to energize the step motor and the controller used to command the movement. It is therefore important to emphasize that in order to meet a specification, it will always be necessary to consider the motor and drive together, as a package (HUGHES; DRURY, 2013).

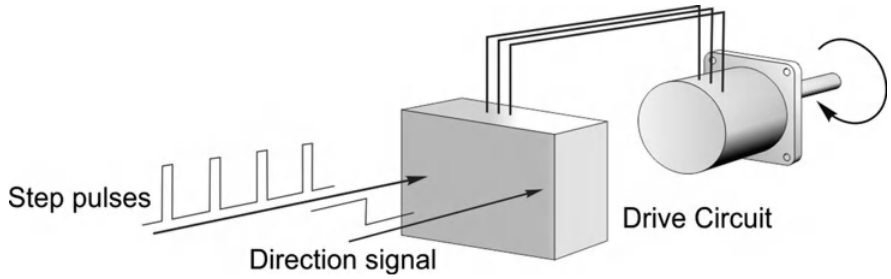

Figure 4: Representative drawing of a step system.
Source: *(HUGHES; DRURY, 2013)*

1.2.1 Open loop x closed loop

Step motors are synchronous motors, in the sense that a pulse of specific length moves the motor by one step. The angle of the step depends on the motor's construction, the most common being a $1.8^o/step$, which is the same of the motor used in this work. Thus, one can establish that a pulse corresponds to a displacement of one step angle $\delta\theta = 1.8^o/step$.

Step motors usually operate in open loop due to the ease of controlling its position by counting the number of pulses sent to the driver. For some specific problems where the load's dynamic is not constant, one can not rely that pulses are not going to be lost along the desired trajectory. A system where there is no guarantee that steps won't be lost should be operated in closed loop with a controller that keeps sending pulses to the

driver, controlling the frequency and direction of movement so the error tolerance will be respected.

Figure 5 presents a diagram of the system in closed loop, where the position is measured and fed back to a closed-loop controller. The driver applies voltages u_a and u_b on phases A and B, respectively, of the step motor and the energizing sequence and its duration dictates the direction and the total displacement of the rotor.

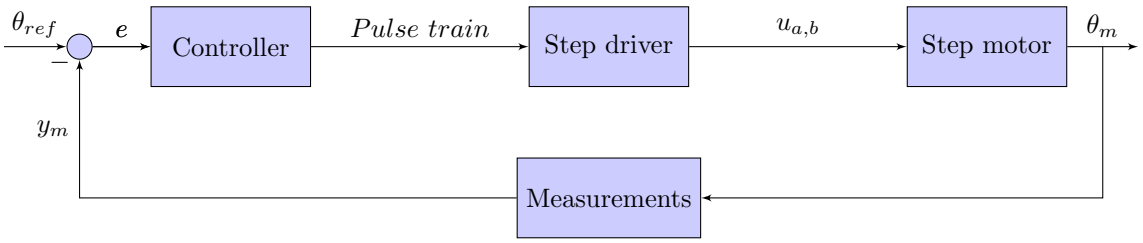

Figure 5: Block diagram of a closed-loop step system.

Source: *The author*

However, step motors tend to drastically loose torque as speed increases, which means that moving a dynamic load at high speeds can be challenging to accomplish even for a closed-loop system. To achieve the desired level of confidence in a high accuracy operation, the systems limit must be well known. Position feedback is a critical aspect on step motors, as the controller may increase the speed to the point where the torque delivered to the axis is lower than the minimum torque required to drive the load. At this point, the micro controller (or PLC) keeps sending pulses to the system, but the mechanics would not respond , leading to an unstable behaviour, thus the importance of position feedback at high speeds step motor operations, in order to detect when the motor starts to stall (e.g. loose steps).

1.3 Related works

In (HENKE et al., 2013) the authors model the saliency between rotor and stator teeth as a variable inductance and shows that it is a function of the rotor angle, providing an accurate model for the hybrid step motor, which can be used to derive more simplified common models (as the one presented is this work). Also, a study on the detent torque (detailed in chapter 2) is performed where a model is proposed and validated. In (MORAR, 2015), the author proposes and validates a model to be used in $Matlab^{©}$ for dynamic simulation. This study presents the hybrid step motors electromechanical equations considering the particularity that the phases are misaligned in such a way that

the model can be used for motors with different number of phases. Several techniques have been used to perform feedback control of a step motor, such as PID, PI, STR (Self Tunning Regulation) and Artificial Neural Networks (KHAN; TAJ; IJAZ, 2014). There are also techniques developed recently that use sensorless estimation of position by measuring the current and the voltage phase of the windings (ACARNLEY; WATSON, 2006), (DRAAMMELAERE et al., 2015), (LIN; CHEN; CAO, 2016).

It is valid to point out that the majority of these control techniques (detailed in section 2.3) control the current of the motor's windings. In (CHUDASAMA; BARIA, 2013) the authors present a low cost topology that also uses voltage to perform speed and torque control. In (users.ece.utexas.edu, 2000), it is shown in details how to choose a proper driver for a step motor and additionally, a complete analysis of the selection process is done. Step motors have also been studied as chaotic systems by non linear dynamic theory as in (ROBERT; ALIN; GOELDEL, 2001), (CORRON et al., 2001) and (PERA; ROBERT; GOELDEL, 2000), where the authors present various solutions for non linear systems and use Feigebaumn diagram and Poincaré sections to identify and characterize them. They apply chaos theory to study step motors behaviour when the speed is increased to a point where the systems starts to become unstable. In (MILADI; FEKI; DERBEL, 2013) the authors propose a novel method using genetic algorithms and neural network based controllers to overcome the chaotic behaviour of a hybrid step motor, where a common "base" PI controller (which could be any other classic controller) is designed to vary the speed of the system and the AI algorithms control when the "base" controller is allowed to change the frequency (speed) to keep the system stable and responsive (i.e, responding to command pulses).

In (LYSHEVSKI, 2014) the author states that an electromagnetically-consistent model is important to ensure optimal energy conversion and proposes a model that assumes a sinusoidal magnetic field for each phase of a hybrid step motor, introducing a magnetic flux ψ_m as a constant (detailed in section 2.2). In (Li; Lu; Shen, 2017) the authors experimentally verify that simplifying the magnetic flux model thus assuming ψ_m constant, does not compromises the performance the step motor model for simulations. In (Dorin-Mirel; Ion; Mihai, 2016) the authors propose an open-loop study of a step system for full and half step driver configurations for different operating frequencies. They do not, however, specify the load conditions and do not show the advantages of using a closed loop step systems, which is one of the goals of this work, to study the behaviour of a step system in open loop for different operating speeds.

The related works presented above analyse the step-by-step performance of the motor

while designing a controller that uses a constant voltage signal as the source power to drive the motor, considering only the equations of the motor, which is not what occurs in practise with the use of step drivers that perform current control by varying the voltage signal via PWM. The effectiveness of the motor's movement depends directly on the drivers capacity of keeping the reference current on the windings, which depends on the proper selection of the components for the *Step System*. Therefore, the importance to study the behaviour of a step motor powered by a step driver.

The proposal of this work is to study together three aspects of a 1 D.O.F robotic arm driven by a step motor controlled by a chopper driver (detailed in section 2.3) when moving a large distance (i.e. $\Delta\theta \geqslant 10 \times \delta\theta$) and under a modelled dynamic load torque ($\tau_L \neq 0$) condition at different speeds. Those three aspects are: i) the motor selection, ii) the performance of the system, iii) the load mass estimation , which cannot be seen in the previous works presented.

1.4 Objectives

This work has three main objectives: i) Define a structured manner for step motor selection, ii) Define a set of parameters to analyse the overall performance of the system, combining both the actuator and the arm models and iii) Find a satisfactory algorithm to estimate the mass of the load. These are detailed next.

Firstly, an algorithm is proposed for step motor selection considering a gear box attached to the motor and the motor's *Speed X Torque* curve. Step motor selection is a gap in industry due to the fact that motors data sheets typically do not present all relevant data and usually comes with very few information regarding the motor's operation parameters, making it difficult to perform a prior analytical understanding of the system. Secondly, an analysis is performed in order to determine the best parameters for operations and a framework is proposed where a set of generic (e.g, in the sense that they are common to all applications) parameters are defined. Since open loop step motors systems are mostly over dimensioned to ensure reference tracking and preventing the motor from stalling (losing steps), this framework is built on the basis of a closed loop system, in order to obtain parameters for step motors operating at their maximum capacity. Thirdly, an algorithm is proposed to estimate the mass of the transported object. The estimation must be done in real-time, during the half coconut transportation from a buffer plate to the paring table. The paring machine is designed to eliminate as least coconut pulp as possible when removing the coconut's skin, so its performance is

measured in percentage of removed material. Therefore, it is of great use to know the mass of the processed coconuts before their processing.

1.5 Structure of the thesis

Chapter 2 presents a review of the different types of step motors and the drivers used to drive them, as well as a common model used for hybrid step motors and a framework for step motor selection. Chapter 3 presents the dynamic model of the arm and combines it with the model of the step motors, deriving the equations of motion for the 1 D.O.F arm system. Chapter 4 presents the framework proposed for optimal operation analysis (including energy analysis, efficiency and time operation) of the system and the mass estimation problem and how it is addressed. Finally, chapter 5 presents the conclusions and possibilities for future works.

1.6 Publications

(SOUZA; COLóN, 2018) was published at CBA 2018 (Congresso Brasileiro de Automática), where the author briefly defines the problem and formulates the framework for step motor selection as well as comparing two controllers using a simplified version of the model presented here. The two different control approaches were a proportional and a H-Infinity controller, used to drive the load through a given $\Delta\theta$. The model of the driver was not initially considered, because the main idea was to first formulate a selection process to determine the best suited step motor for the application.

2 STEP MOTOR FUNDAMENTALS AND CRITERIA FOR SELECTION

This chapter presents the fundamentals of step motors, giving details and a few practical examples when needed, for better understanding regarding the purpose of this work. As well as a proposed approach to select a step motor for a given project.

Step motors present the unique characteristic of moving a very precise and definite angle for each command pulse with high resolution, for most commercially motors available, up to $\delta\theta = 0.007^{o}$ when a motor of 1.8^{o} per step is configured with a micro stepping rate of 1/256. This chapter describes the main types of step motors, focusing on the hybrid type which was chosen for this work, the electromechanical model for the step motor, the drivers that are mostly used in *Step Systems*, concluding with a framework for step motor selection. It can be briefly described as a synchronous electrical machine which moves in a well defined angle, here called step angle and represented by $\delta\theta$, according to the excitation sequence on its windings. The torque produced depends on the current of the windings and the electromagnetic characteristics and the rotor's position, as detailed in section 2.2.

It is important to be familiar with a few concepts regarding step motors torque, described bellow (MELKEBEEK, 2018):

- **Static characteristics**

  Holding torque: It is the torque exerted by the motor under non-zero current and zero load torque;

  Detent torque: It is the torque exerted by the motor under zero current and zero load torque;

- **Dynamic characteristics**

  Pull-in torque: It gives the range for the load torque as a function of frequency, in which the step motor will start from rest and not stall;

Pull-out torque: It gives the range for the load torque as a function of frequency, in which an already running, at constant speed, step motor will not stall (loose steps).

The step driver selection is essential to extract maximum performance of a given step motor and should also consider the motor's wiring due to the fact that the drivers are designed for specific modes of operation to achieve optimized performance, as detailed in section 2.3.1.

2.1 Types of step motors

2.1.1 Permanent magnet

This type of motor consists of a solid, axially magnetized rotor which turns when a winding is excited, attracting the south pole and producing a 90º degree rotation on the axis. Figure 6 shows a full *clockwise* turn excitation sequence "$A \rightarrow B \rightarrow A' \rightarrow B \rightarrow A$" for the Permanent Magnet step motor. The order of excitation of the windings determines the direction of rotation, for example to turn the motor *counterclockwise* the sequence would be: "$A \rightarrow B' \rightarrow A' \rightarrow B \rightarrow A$".

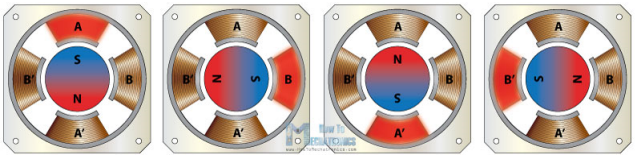

Figure 6: Permanent magnet step motor excitation sequence.
Source: *(Dejan Nedelkovski,)*

2.1.2 Variable reluctance

This type of construction consists of a non-magnet soft iron toothed rotor that rotates when current flows through one winding to keep minimum air gap between the rotor and the stator. Its step size is usually greater than other types (ACARNLEY, 2002). Figure 7 shows the stator and rotor arrangement for a 3 phase ($\delta\theta = 30^o$) variable reluctance step motor. When current flows through phase A, the rotor is aligned with its stator poles as shown on Figure 7(a), then when current flows through phase B, the rotor turns 30^o as in 7(b), and another 30^o when phase C is energized.

To control the direction of movement, one simply control which phase will be energized first For example, the sequence "$A \rightarrow B \rightarrow C \rightarrow A$" rotates the motor clockwise,

whereas the sequence "$A \rightarrow C \rightarrow B \rightarrow A$" rotates the motor counterclockwise. In this type of motor, current flows through the winding, regardless its direction, and the motor will turn a step. This mode of operation is known as "1-phase-on", and is the simplest way of making the motor step (HUGHES; DRURY, 2013).

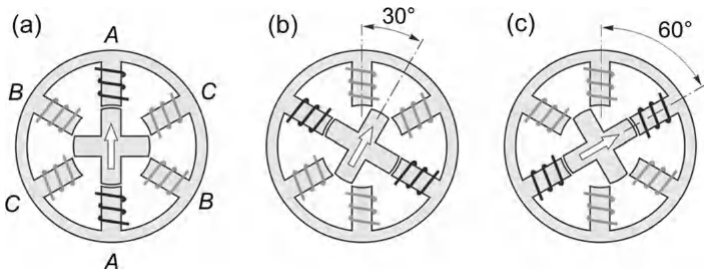

Figure 7: Variable reluctance motor axis section.

Source: *(HUGHES; DRURY, 2013)*

2.1.3 Hybrid step motor

A hybrid step motor is a combination of the permanent magnet and the variable reluctance motors, having magnetized toothed rotor and stator. It often provides a smaller step angle. Most hybrid step motors present $\delta\theta = 1.8^{o}$. The axis construction is different from the PM, and is made of two sections of magnet: the south pole and the north pole with an offset of one tooth between them (HUGHES; DRURY, 2013). Figure 8 shows a section perpendicular to the axis of the hybrid motor. The colors yellow and red represent, respectively, the north and south poles of the rotor. The driving sequences and types for the hybrid step motor are detailed in section 2.3.

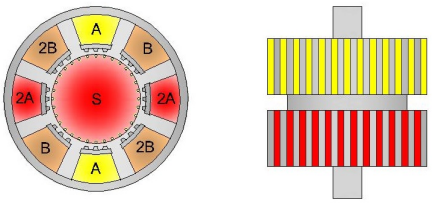

Figure 8: Hybrid step motor side and top views

Source: *The author*

2.2 Step motor model

In (MORAR, 2003), the author shows the electromechanical equations for the step motor and in (LYSHEVSKI, 2014) the author proposes to model the step motor in a

similar manner, but using the magnetic flux ψ_m as a constant to simplify the model. For a two phase hybrid step motor, the total torque is given by (LYSHEVSKI, 2014):

$$\tau_m = \psi_m[-i_a(t)sin(n\theta_m(t)) + i_b(t)cos(n\theta_m(t))], \tag{2.1}$$

where:

- n is the number of rotor's pole pairs;
- ψ_m is the magnetic flux of the motor
- $i_a(t)$ and $i_b(t)$ are the currents on phases "A" and "B", respectively;
- $\theta_m(t)$ is the angular position of the rotor.

The relation between the voltage and current on the coils is given by Equation 2.2 for the *j-th* phase:

$$u_j = \text{emf}_j + Ri_j(t) + L\frac{di_j(t)}{dt}, \tag{2.2}$$

where:

- R is the resistance of the coils;
- L is the inductance of the coils;
- u_j is the voltage applied on phase "j";
- i_j is the current of phase "j";
- emf_j is the induced electromotive force on phase "j", given by Equation 2.3 (MORAR, 2003):

$$\text{emf}_j = \psi_m sin(n\theta(t) + \phi_j)\dot{\theta_m}(t), \tag{2.3}$$

where, $\dot{\theta_m}(t)$ is the angular velocity of the rotor and ϕ_j is the position of phase $j = \{0, 90^o\}$.

Equation 2.1 shows that the total torque produced by the step motor alone does not depend on the angular velocity but rather of the current and the rotor's position. As stated in section 2.3, the torque of the complete *Step System* is a function of the motors speed because it will influence its capacity of reaching the desired current, thus affecting the delivered torque.

The magnetic flux ψ_m is an uncertainty since it is not specified by manufacturers and depends on the construction and assembly of the motor as well as on the operating conditions, as the magnetic properties of the iron core may vary with temperature. For simplicity, this work assumes that it is constant. It can also be obtained experimentally, by driving the motor at constant speed and measuring the maximum open circuit winding voltage E_m. The magnet flux can then be calculated by Equation 2.4 (*Mathworks*©, 2007):

$$\psi_m = \frac{30}{n\pi}\frac{E_m}{N}, \tag{2.4}$$

where, n is the number of rotor pole pairs, m is the number of phases and N is the speed in *rpm*.

Combining the mentioned equations ((MORAR, 2003) and (LYSHEVSKI, 2014)), the two phase hybrid step motor model can be described as:

$$\begin{aligned}
\ddot{\theta_1}(t) &= \frac{\psi_m[-i_a(t)sin(n\theta_m(t)) + i_b(t)cos(n\theta_m(t))] - B\dot{\theta}_m(t) - \tau_L}{J}, \\
\dot{i_a}(t) &= \frac{u_1(t) + \psi_m sin(nx_1(t))\dot{\theta}_{1(}t) - Ri_a(t)}{L}, \\
\dot{i_b}(t) &= \frac{u_2(t) - \psi_m cos(nx_1(t))\dot{\theta}_{1(}t) - Ri_b(t)}{L},
\end{aligned} \tag{2.5}$$

where:

- τ_L is the load torque.
- J is the moment of inertia of the system.
- B is the viscous damping coefficient

2.3 Step motor driving

The two most common ways of driving a step motor is using either a unipolar driver (current flows in one direction) or a bipolar driver (current flows in both directions). The first requires less circuitry and is simpler to operate. The latter is the most common driver used nowadays, even though it requires a more complex circuitry, due to the ease of using all-in-one IC's.

Bipolar driver main advantage over unipolar driver is that the first can generate more

torque due to the possibility of keeping both phases energized at the same time (HUGHES; DRURY, 2013). Figure 9 shows the circuit for unipolar and bipolar driving, respectively. One can see a single single transistor (usually a MOSFET) for each coil of the motor from a common $V+$ power source to the ground and a full H-bridge for each phase (2 coils in parallel) of a step motor. As stated previously, the full-bridge circuit is far more complex to drive and control. It provides however, more flexibility to the operation, making it more interesting also, because it can be deployed more easily with today's technology.

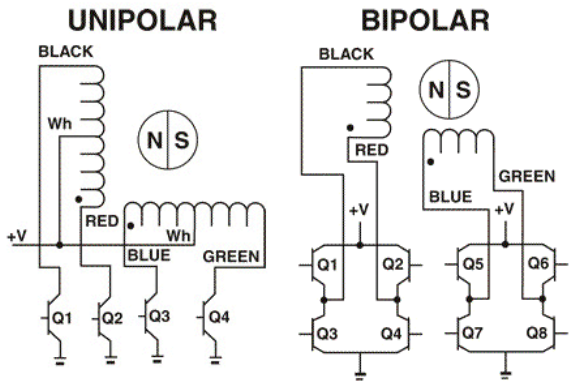

Figure 9: Bipolar and unipolar driver circuits.

Source: *(George, 2012)*

To operate a step motor with the appropriate driver, one needs simply a pulse generator and the driver will energize the motor's coils accordingly, to achieve the desired positioning sequence, using either full step, half-step or micro-stepping positioning excitation modes.

The excitation mode will influence directly on the torque ripple. According to (Deraemmelaere et al., 2015) the smaller the step, the smaller the ripple and the smoother the movement will be. However, in micro stepping excitation mode, the current will rise in a sinusoidal manner quantized by the number of steps, as shown in Figure 10c. This means that the current will rise to its nominal value slowly and if the current is too small, the system might not move properly depending on the load torque. This situation may cause the motor to loose steps and stall. However, if the motor does not need maximum current to surpass the load torque, the micro-step mode will increase the current proportionally to the micro-stepping rate until it reaches the current reference value. This will cause the motor to reach the smaller currents faster as between steps, the current will start from a non zero value, diminishing the effect of the windings inductance.

Figure 10 shows the current on the phases of a step motor with a maximum reference current of $6.0A$ and angular speed $\omega = 0.7854\ rad/s$ simulated in the *power steppermotor* model from $MatLab^{©}$ which represents a step model energized by a bipolar step driver

with a DC power source. The dashed vertical lines represent a single step of $\delta\theta = 1.8^{o}$. It is possible to see that energizing all the coils for a full sinusoidal cycle (both phases with positive and negative current) corresponds to $4\delta\theta = 7.2^{o}$ of displacement. A full turn of 360^{o} corresponds to $\frac{360}{7.2} = 50$ sinusoidal cycles, that corresponds to the 50 rotor teeth of the step motors.

For the full-step mode presented in Figure 10a, only one of the phases is energized at a given time, whereas for the half-step and micro-stepping modes, shown, respectively, in Figures 10b and 10c, both phases are energized at a given time, achieving maximum torque. The difference between them is the resolution. In Figure 10b each command pulse represents $\delta\theta = 0.9^{0}$ of rotation and in Figure 10c each command pulse represents $\delta\theta = 0.225^{0}$ of rotation, which allows a more precise positioning.

- **Full step:** The motor turns its nominal resolution of $\delta\theta$.
- **Half step:** The motor turns half of its nominal resolution $\frac{\delta\theta}{2}$.
- **Micro stepping:** The motor turns $\frac{\delta\theta}{n}$ of its nominal resolution, where n is the rate for the micro stepping mode, normally power of 2.

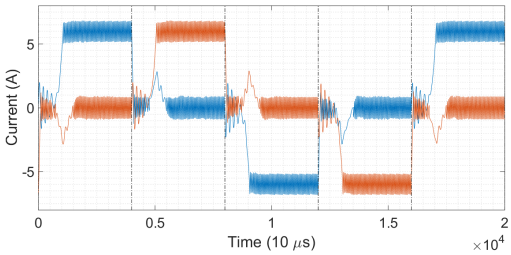

(a) Full step drive

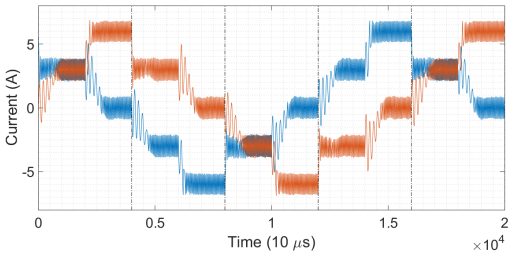

(b) Half step drive

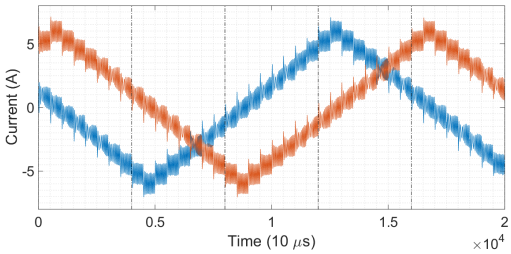

(c) Microstepping drive

Figure 10: Step motor different excitation modes.

Source: *The author*

2.3.1 Driver operation types

The step motor is essentially a discrete motion machine where its windings must be excited in a proper manner at a proper time. The step motor's driver, a chopper-driver type for this work, ensures that this task is performed efficiently so that the users can design motion algorithms considering only a pulse train delivered to the driver and the measured angle and velocity.

The driver is a dedicated part in a *Step System*, designed to provide the current to the windings from the power source. It does not possess the features to track and/or correct position and speed errors. It is commonly a translator of pulses into energy, which will then generate motion on the rotor. In (HUGHES; DRURY, 2013), the author defines three types of driver in unipolar circuitry for simplicity, explained below.

2.3.1.1 Constant-voltage driver

The simplest driver operation consists of a constant voltage power supply designed to reach the motor's rated current (given by the manufacturer) at steady state after several times-constants of L/R, which is the time constant of the RL circuit of each phase. Figure 11 shows a simple circuit example.

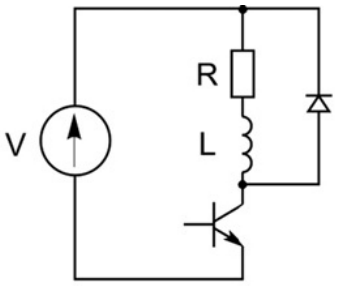

Figure 11: Constant voltage driver circuit example.

Source: *(HUGHES; DRURY, 2013)*

At low step rates, this provides a very well defined first order current curve which will rise to the rated current when the MOSFET is turned *on* and will decay to zero when the MOSFET is turned off for every command pulse. This implies that at high stepping rates, the decay time of the current may be slower than the pulses frequency, which means that a new command will arrive before the current reaches zero or its rated value and the MOSFET will be turned on again, making a toothed shape current curve, where the current is never off when it is supposed to be and does not reaches its reference value, as shown in Figure 12. The torque delivered in this condition is reduced and might be

negative when there is current on a phase supposed to be turned off.

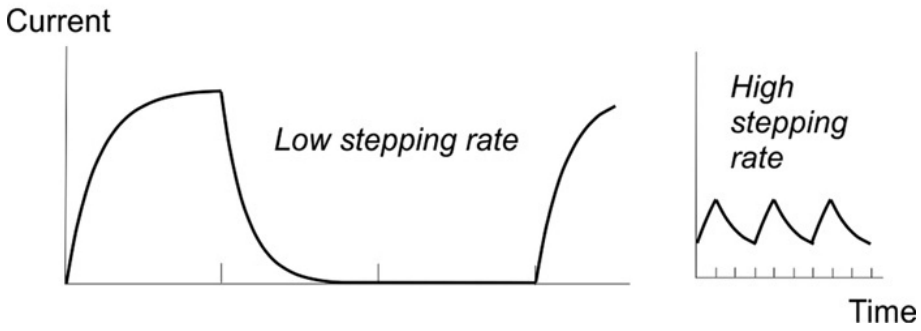

Figure 12: Constant voltage waveform example.

Source: *(HUGHES; DRURY, 2013)*

2.3.1.2 Current-forced driver

It works similar to the constant-voltage driver, but it uses an extra resistor to keep the rated current within the specified range, shown in Figure 13, while increasing the power supply voltage in order to reach the rated current faster when the MOSFET is *on*.

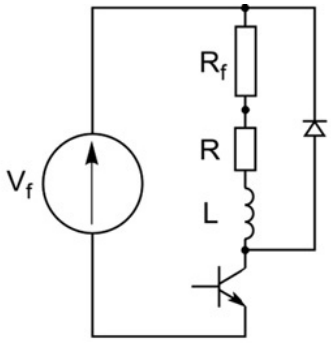

Figure 13: Current-forced driver circuit example.

Source: *(HUGHES; DRURY, 2013)*

Even though it prevents the toothed wave form from the previous driver, as shown in Figure 14, its main disadvantages is inefficiency and the need of a high power supply. When the motor is stopped with current flowing though the windings, this leads to overheating the forcing resistors. This extra heat can lead to cooling problems within a system if it is not dealt properly. The resistance of the extra resistor is usually 2 to 10 times the resistance of the winding.

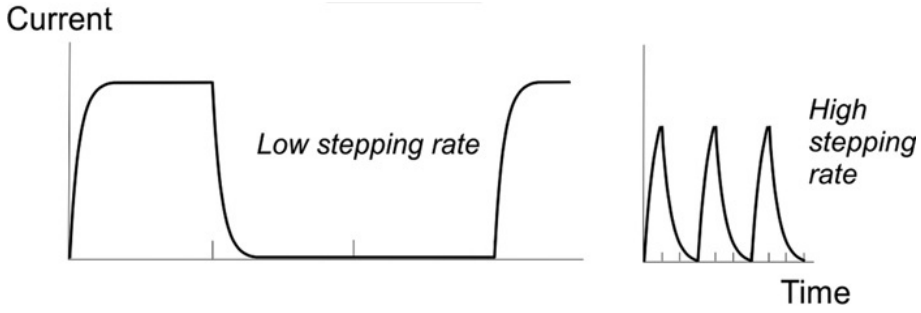

Figure 14: Current-forced wave form example.

Source: *(HUGHES; DRURY, 2013)*

2.3.1.3 Constant current (chopper driver)

This arrangement uses a high voltage power supply to obtain fast changes in current when the phases change state and operates in a closed loop fashion, thus reducing the effects of the back electromotive force. Figure 15 shows a circuit example for one half of a H-Bridge required for each phase of the hybrid motor.

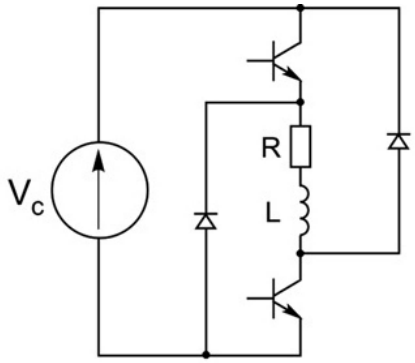

Figure 15: Chopper driver circuit example.

Source: *(HUGHES; DRURY, 2013)*

The lower MOSFET remains turned *on* during the entire period in which current is required, whereas the upper MOSFET is switched *on* when the current drops below a specified threshold around the rated current, so the current curve will looks like the curves on Figure 10. When the stepping rate (i.e. speed) rises to a point where the MOSFET's *on* period is smaller than the current rise time, the current never reaches its reference value and the driver becomes a constant voltage driver, dropping the *pull-out* torque drastically. Figure 16 shows that this driver has the closest operation to an ideal rectangular current wave form.

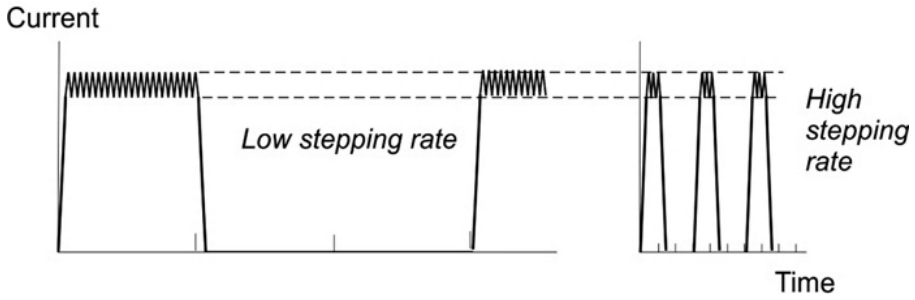

Figure 16: Chopper driver wave form example.

Source: *(HUGHES; DRURY, 2013)*

The three driver types explained previously show that step motors always tend to never reach the rated current when the stepping rate rises to the points where the *on* period of the driver is smaller than the L/R time constant of the motor, thus leading to a rapid descend in the *pull-out* torque delivered by the rotor.

This is the reason why step motors torque drops as speed rises, and this $TorqueXSpeed$ curve depends on the motor, the driver, the excitation mode and the power supply. It is not a closed formula and is usually presented in the data sheets on a limited number of tested parameters, that is, the manufacturers do not present this information with sufficient data, so costumers do not have many options to work with when designing an application. For example, Figure 17 shows the $TorqueXSpeed$ curve for the motor model KTC-HT34-487, where the manufacturer shows two curves for different stepping rate values, but does not say, however, at which voltage these curves where obtained (usually for NEMA34 size motors, the voltage is 24/48 VDC, but it is not guaranteed). Another example, from the same manufacturer, is the motor model KTC-110HS165, shown in Figure 18, where the voltage is specified as 80 VDC, however no micro stepping rate information is given.

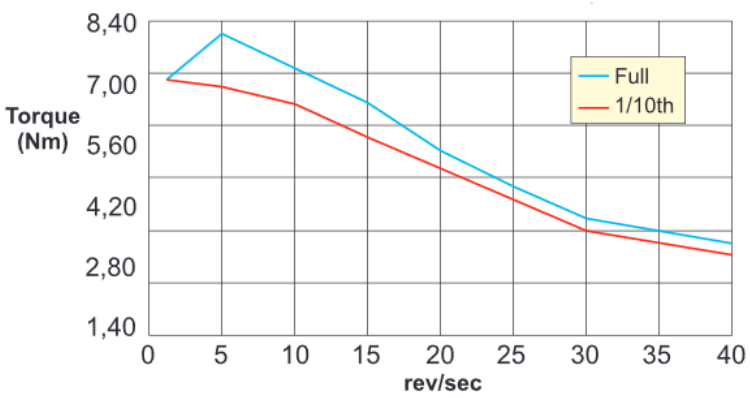

Figure 17: $TorqueXSpeed$ curve for the motor KTC-HT34-487.

Source: $Kalatec^{©}$

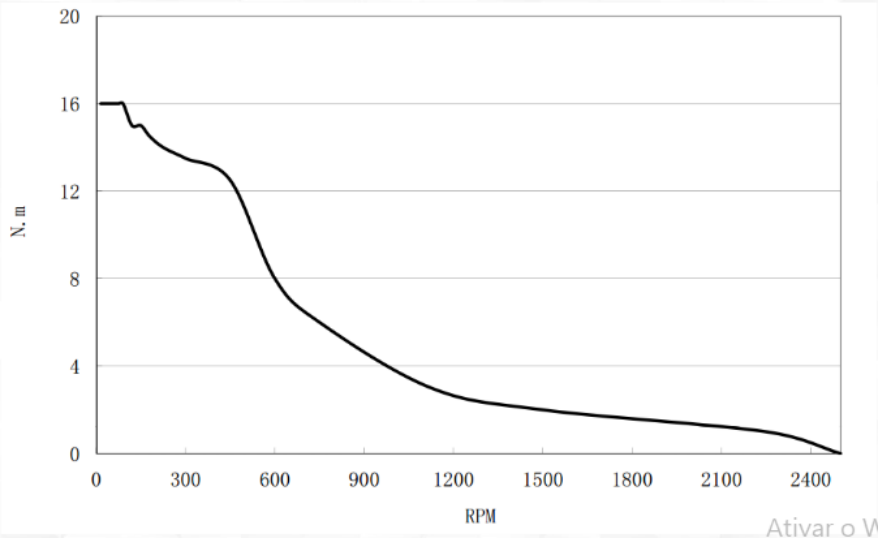

Figure 18: *TorqueXSpeed* curve for the motor KTC-110HS165.

Source: *Kalatec*©

These inconsistencies in step motor manufacturers data sheets, makes it difficult to arrive at a precise conclusion upon specification, specially because it is not possible to guarantee, from the documentation available, the torque of a given motor at the desired speed for the application, given all the application operation conditions, such as: supply voltage, rated current, micro stepping rate, load torque and speed.

2.4 The γ factor

To choose the step motor for an application one must consider its *TorqueXSpeed* limitations. The motor can stall and loose synchronism due to disturbances or a change in the load's torque, for example. To overcome this problem, one must select a motor with higher torque. The question is: *how much higher?*

The γ factor is used to quantify the previous question and is in practice greater than one. It regulates the maximum torque that needs to be delivered by the motor, specifying a new requirement to motor selection. Defining τ_f as the torque needed to move the load and τ_m the torque of the motor, Equation 2.6 gives the new value to be pursued when selecting the motor:

$$\tau_m = \gamma \tau_f. \tag{2.6}$$

2.5 Step motor selection

Several technical features need to be considered in the process that will result in the right step motor for the application: i) Driver selection, ii) Programming platform (PLC x Microcontroller), iii) Physical space, iv) Total cost, v) Speed x Torque. The correct choice will provide a system that delivers the maximum torque, without overloading and preserving its full lifetime. In the following, we present the criteria used to select the driver and the gearbox.

2.5.1 Driver selection

When using an encoder to read the position feedback from the axis in a system with gearbox, it is necessary to compare the encoder's resolution and the backlash (i.e. the gap between mechanical parts of a system in which one part moves towards the next without applying force to it) from the gearbox. If the encoder resolution is higher than the backlash, the closed loop system will naturally try to compensate the backlash all the time, wasting power to perform an error correction that can not be accomplished, due to the system's dynamics. To avoid this, one should first estimate the gearbox backlash and either select an encoder with lower resolution or include a minimum error tolerance in the controller before it actuates.

According to Equations 2.1 and 2.2, the higher the current on the windings, the higher the torque, and the higher the supply voltage, the higher is the torque (Geckodrive Motor Controls (GMC), 2010). On the case study presented in this work, the driver selected is a PCB (Printed Circuit Board) driver with external power MOSFETs, and a 48 VDC supply voltage.

2.5.2 Gearbox selection

The gearbox is a resource widely used by many applications, as it multiplies the torque on the shaft. But to achieve this, it imposes a speed reduction on the motor. The gearbox reduction rate is defined in Equation 2.7:

$$\eta = \frac{\omega_m}{\omega_f}, \tag{2.7}$$

where ω_m is the speed of the motor and ω_f is the desired speed.

The gearbox chosen for this case study is a worm gearbox type, as shown in Figure

19, with speed reduction of $1:7.5$, meaning that the motor must run 7.5 times faster to achieve the desired speed. The backlash of the gearbox, which stands for how much the input axis will move before the engines inside the gearbox actually touches the next teeth and produce movement to output shaft, is 45 $arcmin \equiv 0.75^o$, which is less than the output's resolution of $1.8^o/step$, in order to not generate a pulse at the encoder when the backlash is at its maximum.

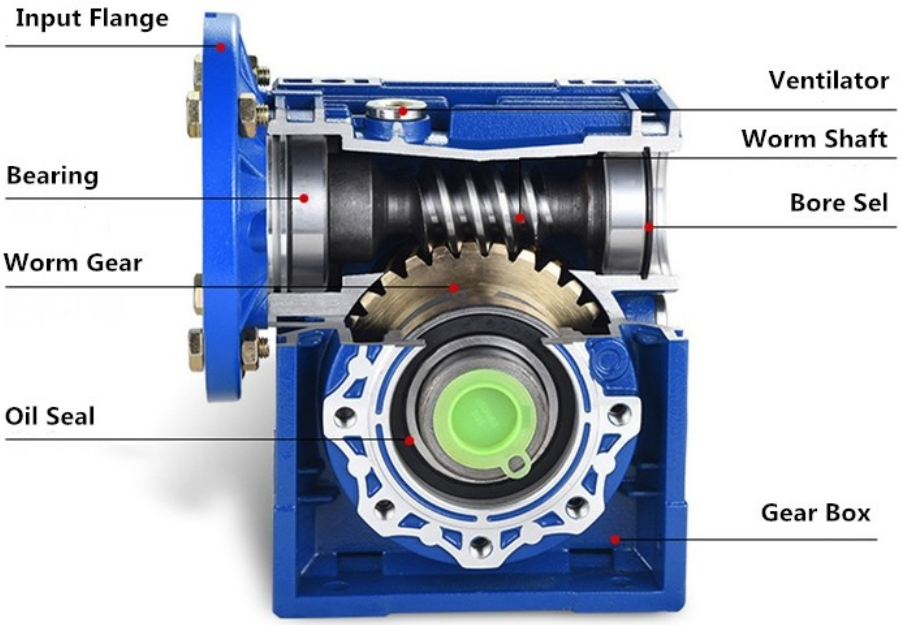

Figure 19: Worm gearbox detail.

Source: *DEVO GearDrive*©

2.5.3 Step-by-step guide of step motor selection

Figure 20 shows an example of a $TorqueXSpeed$ curve for the motor $86HS82-4504A14-B35-02$ (*by Policomp*©). The given curve was obtained by the manufacturer using a 48 VDC power source, 4.45 A current, and 1/8 micro stepping configuration. Since the curve presented by the manufacturer is obtained empirically under different operating conditions, it would be impractical to precisely estimate the $Torque \times Speed$ relation to the desired operating conditions for each candidate motor.

To find the motor that fits the requirements, one should essentially estimate the motor curve on the desired operation conditions and verify whether the selected motor has the required torque at the required final speed. In order to select the motor-gearbox setup, Equation 2.8 must be satisfied:

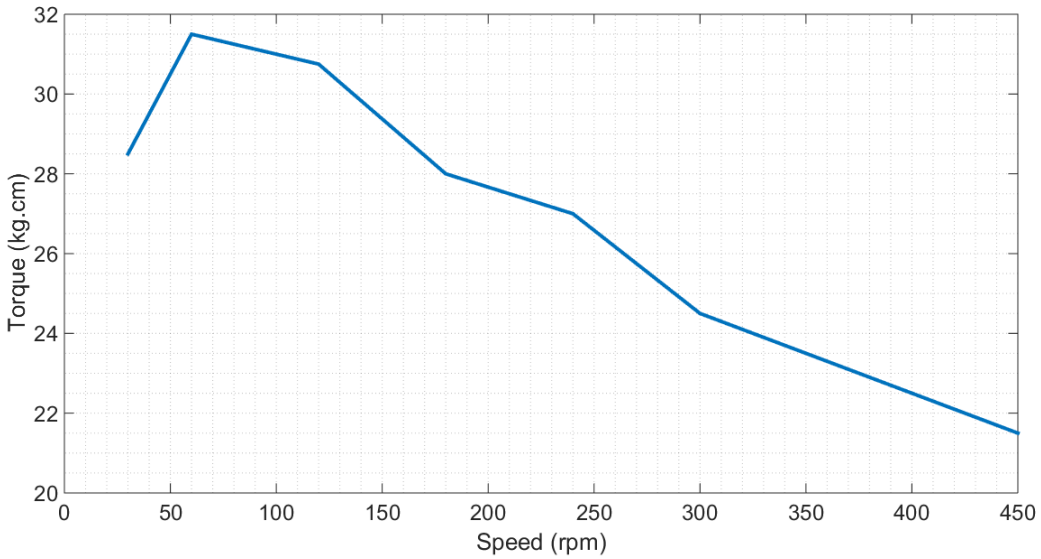

Figure 20: *TorqueXSpeed* graph of the step motor 86HS82-4504A14-B35-02
Source: *The author*

$$\tau_m \eta > \gamma \tau_f. \tag{2.8}$$

where τ_m is the torque of the motor, τ_f is the required torque to the axis, η is defined in Equation 2.7, and γ is defined in Equation 2.6. The value of γ must be either 1.3 or 1.5 (those values are explained in the following). If Equation 2.8 is not satisfied, the setup must be changed. The γ factor is imperative to establish robustness of the application. The author proposes a linear estimation for voltage supply starting from the provided curve and then multiplied by a factor $\gamma = 1.3$ (this value is encouraged to be used with a closed loop. If the system works in open loop, the authors recommend a value of $\gamma = 1.5$). The value $\gamma = 1.3$ has been validated in practice to be a good choice for this application. This factor is to perform secure operation without stalling the motor during the process, because if $\gamma = 1$ is chosen and the motor stalls, even with an feedback system, and if the machine is operating within unusual conditions, the controller might not be able to prevent unstable behaviour.

Most of manufactures provide only one graph for each motor, and to arrive in a consensus of what motor to choose, estimations need to be made based on the information given in the data sheets. For example, the behaviour of the $Torque \times Speed$ curve with a different power supply has direct influence on the output torque and power delivered by the motor (Geckodrive Motor Controls (GMC), 2010). These estimations need to be done very carefully, since motor performance changes from one driver to another, as well as with other parameters, such as resonance and inertia (users.ece.utexas.edu, 2000).

We propose a step-by-step guide to select a step motor for a given application:

1. Calculate the torque needed on the axis, τ_f;
2. Define technology (PLC or microcontroller) to be used on the project;
3. If the system will operate in closed-loop, with position feedback from an encoder, then go to 4. If the system is open-loop, then go to 5;
4. Define $\gamma = 1.3$, then go to 6;
5. Define $\gamma = 1.5$, then go to 6;
6. Estimate the maximum speed of operation;
7. Select a step motor and/or a gearbox, and calculate τ_m by using the $speed \times torque$ graph (like in Figure 20).
8. If Equation 2.8 is met, then go to 10, else go to 9
9. Compare the *speed X torque* curve of the motor with the relations available for the chosen gearbox and evaluate if the motor, the gearbox or both should be changed, then go back to 7.
10. Test the motor/gearbox setup on site and verify whether all the necessary variables were considered in step 1. If the test is successful, then the process is complete, otherwise go to 1.

The process of estimating the behaviour of the motor is a trial and error process (users.ece.utexas.edu, 2000). The author proposes that the designers consider a linear relation from the manufacturer's information when varying the parameters within a small range and start the trial process. This range, however can vary within the same motor under different operation conditions.

3 THE ROBOTIC ARM

This chapter presents the mathematical model for the 1 DOF robotic arm analysed in this work together with an equilibrium analysis.

3.1 Equations of the arm

The arm's dynamic equations are derived below, as shown in Figure 21. Considering a rigid body of length L_1 with a mass m_g concentrated at the tip, θ_1 the angle measured from the horizontal axis (*x axis*) and the base of the body as the reference frame origin, the end effector coordinates in function of the joint coordinate are presented in Equation 3.1. Differentiating it in relation to time, we find the velocity vector, described in Equation 3.2.

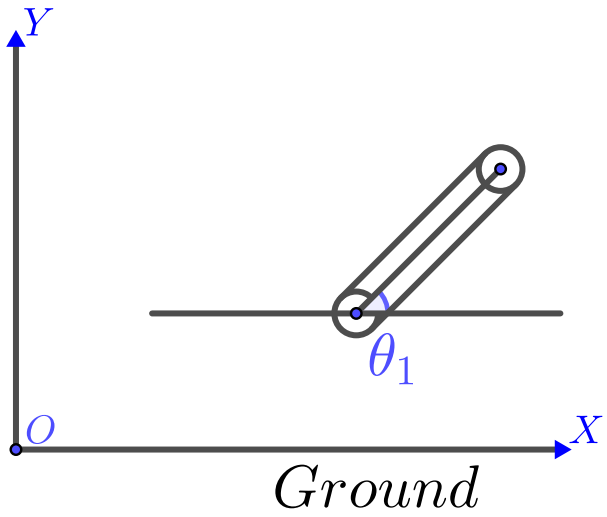

Figure 21: Robotic arm.

Source: *The author*

$$\begin{aligned} x_1(t) &= L_1 cos(\theta_1(t)), \\ y_1(t) &= L_1 sin(\theta_1(t)), \end{aligned} \tag{3.1}$$

$$\begin{aligned} \dot{x_1}(t) &= -\dot{\theta_1}(t) L_1 sin(\theta_1(t)), \\ \dot{y_1}(t) &= \dot{\theta_1}(t) L_1 cos(\theta_1(t)), \end{aligned} \tag{3.2}$$

$$\mathbf{v(t)} = \begin{bmatrix} \dot{x_1}(t) \\ \dot{y_1}(t) \end{bmatrix}.$$

The velocity vector can be squared, as shown in Equation 3.3, and then used to calculate the systems kinetic energy in Equation 3.4:

$$\begin{aligned} \mathbf{v(t)}^2 = ||\mathbf{v(t)}||^2 = \mathbf{v(t)}^T \mathbf{v(t)} = \\ \begin{bmatrix} -\dot{\theta_1}(t) L_1 sin(\theta_1(t)) & \dot{\theta_1}(t) L_1 cos(\theta_1(t)) \end{bmatrix} \begin{bmatrix} -\dot{\theta_1}(t) L_1 sin(\theta_1(t)) \\ \dot{\theta_1}(t) L_1 cos(\theta_1(t)) \end{bmatrix} \\ = \dot{\theta_1}^2(t) L_1^2, \end{aligned} \tag{3.3}$$

$$K = \frac{1}{2} m v^2 = \frac{1}{2} m_g \dot{\theta_1}^2(t) L_1^2. \tag{3.4}$$

The potential energy is shown in Equation 3.5:

$$U = mgh = m_g g L_1 sin(\theta_1(t)). \tag{3.5}$$

Both potential and kinetic energies are used to calculate the Lagrangian defined in Equation 3.6:

$$\mathscr{L} = K - U = \frac{1}{2} m_g \dot{\theta_1}^2(t) L_1^2 - m_g g L_1 sin(\theta_1(t)), \tag{3.6}$$

and used in the Euler-Lagrange equation to calculate the load torque τ_L of the arm, as in Equation 3.7 (SPONG; HUTCHINSON; VIDYASAGAR, 2005):

$$\begin{aligned} \tau_L &= \frac{d}{dt} \frac{\partial \mathscr{L}}{\partial \dot{\theta_1}} - \frac{\partial \mathscr{L}}{\partial \theta}, \\ \tau_L &= \ddot{\theta_1} m_g L_1^2 - m_g g L_1 cos(\theta_1(t)). \end{aligned} \tag{3.7}$$

Equation 3.7 shows that the torque exerted by the arm depends on the inertia of the

arm as a rigid body and on a sinusoidal term, meaning that the load torque depends on the arm's position. It can also de used to calculate the maximum torque required to move the load from rest (when the arm is not carrying any load)):

$$\tau_L = \cancelto{0}{\ddot{\theta}_1 m_g L_1^2} - m_g g L_1 \cancelto{1}{cos(\theta_1)}, \tau_L = -m_g g L_1 = 1.4024\ Nm, \tag{3.8}$$

where:

- $m_g = 0.530kg$
- $L_1 = 0.270m$
- $g = 9.8m/s^2$

Equation 3.8 can be used as the τ_f value described in step one of section 2.5.3, by adding an estimation of the heaviest coconut to the the value of m_g.

3.2 Mathematical model for the complete mechanical system

The torque of the step motor, τ_m, must be equal to or greater than the load torque in order for the system to move, from which one can derive Equation 3.9.

$$\tau_m = \ddot{\theta}_1 m_g L_1^2 - m_g g L_1 cos(\theta_1(t)) + B\dot{\theta}_1(t). \tag{3.9}$$

Combining Equation 3.9 of motion and Equation 2.5 of the step motor, a state space model with four state variables can be derived to represent the system in the continuous time domain. This combination is straight forward in this approach since the angle of the arm is the same as the angle of the motor shaft, that is, $\theta_1 = \theta_m$.

Electing the state variables as: i) $x_1(t) = \theta_1(t)$, the arm's angle, ii) $x_2 = \dot{\theta_1}(t)$ the arm's speed, iii) $x_3(t) = i_a(t)$, current on phase "A" and iv) $x_4(t) = i_b(t)$, current on phase "B", the combined equations written in form of state variables are presented in Equation 3.10:

$$
\begin{aligned}
\dot{x_1}(t) &= x_2(t), \\
\dot{x_2}(t) &= \frac{\psi_m[-sin(nx_1(t))x_3(t) + cos(nx_1(t))x_4(t)] + m_g g L_1 cos(x_1(t)) - Bx_2(t)}{J_L + J_m}, \\
\dot{x_3}(t) &= \frac{u_1(t) + \psi_m sin(nx_1(t))x_2(t) - Rx_3(t)}{L}, \\
\dot{x_4}(t) &= \frac{u_2(t) - \psi_m cos(nx_1(t))x_2(t) - Rx_4(t)}{L},
\end{aligned}
\tag{3.10}
$$

where:

- J_m is the moment of the inertia of the motor.
- J_L is the moment of inertia of the load.

The control inputs are: i) $u_1(t)$, voltage on phase "A" and ii) $u_2(t)$, voltage on phase "B" with all states measured, hence the output is $\mathbf{y(t)} = [x_1(t)\ x_2(t)\ x_3(t)\ x_4(t)]$. These equations form a nonlinear system with 4 measured state variables where the main objective is to control the position and velocity of the arm. The load inertia of the arm is given by Equation 3.11:

$$J_L = m_g L_1^2. \tag{3.11}$$

The system uses a gearbox as described in section 2.5.2 with ratio 1 : 7.5, applying the value of $\eta = 7.5$ to J_L gives the actual moment of inertia J_1 felt by the motor, described in Equation :

$$J_1 = \frac{J_L}{\eta^2} = \frac{m_g L_1^2}{7.5^2} = 0.00068\ kgm^2. \tag{3.12}$$

The chosen value of the rotors inertia of the step motor is $J_m = 2.7 \times 10^{-}4\ kgm^2$, which represents 39% of the moment inertia J_1 sensed by the motor. The total moment of inertia of the systems is given by Equation 3.13:

$$J_{tot} = J_1 + J_m. \tag{3.13}$$

3.2.1 Equilibrium analysis

Whereas a complete *Step System* operates essentially in a discrete manner, the equations in the continuous time domain are, however, important to perform equilibrium analysis in order to understand the system's general behaviour. Considering the left side of equation 3.10 equal to zero (equilibrium state) and electing the variable ρ as a constant defined by Equation 3.14:

$$\rho = \frac{m_g g L_1}{\psi_m}, \tag{3.14}$$

one wants to fix three different equilibrium points and starting by analysing state variable $\dot{x_2}(t)$ from Equation 3.10:

1. $\mathbf{x_1 = 0^o}$: (position "Unload" from Figure 2)

$$\begin{aligned} &- \cancelto{0}{sin(0)}\, x_3 + \cancelto{1}{cos(0)}\, x_4 = -\rho \cancelto{1}{cos(0)} \\ &x_4 = -\rho, \\ &u_2 = R x_4 \;\rightarrow\; u_2 = -R\rho, \\ &u_1 = R x_3. \end{aligned} \tag{3.15}$$

   Since only the torque from phase "B" is actuating on the shaft at this position, $x_3 = 0 \;\therefore\; u_1 = 0$. Considering the driver is able to maintain constant current, the voltage (control) needed to hold the arm at $\theta_1 = 0^o$ is $u_1 = 0$ and $u_2 = R\rho$.

2. $\mathbf{x_1 = 90^o}$:

$$\begin{aligned} &- \cancelto{1}{sin(90)}\, x_3 + \cancelto{0}{cos(90)}\, x_4 = -\rho \cancelto{0}{cos(90)} \\ &x_3 = 0, \\ &u_1 = R x_3, \\ &u_2 = R x_4. \end{aligned} \tag{3.16}$$

   Only the torque from phase "A" is actuating on the shaft at this position, implying that $x_4 = 0 \;\therefore\; u_2 = 0$. The load torque $\tau_L = 0$, making the current $x_3 = 0$. The current of both phases "A" and "B" are zero, thus no torque is necessary to hold the arm at $\theta_1 = 90^o$, hence $u_1 = 0$ and $u_2 = 0$. This point is the natural equilibrium point of the system, that is, no control effort is necessary to hold the system at this state. But it is a unstable equilibrium, and only a closed loop system can transform this point in a stable equilibrium point.

3. $\mathbf{x_1 = 30^o}$:

$$\begin{aligned} &\cancel{-sin(30)}^{\frac{1}{2}} x_3 + \cancel{cos(30)}^{\frac{\sqrt{3}}{2}} x_4 = -\rho \cancel{cos(30)}^{\frac{\sqrt{3}}{2}} \\ &x_3 - \sqrt{3}x_4 = \sqrt{3}\rho, \\ &u_1 = Rx_3, \\ &u_2 = Rx_4. \end{aligned} \tag{3.17}$$

Considering that the driver is able to maintain constant current, the voltage, on both phases, necessary to hold the arm at $\theta_1 = 30^o$ is: $u_1 = Rx_3$ and $u_2 = Rx_4$.

From Equation 3.17, one can generalize that for any given stationary angle, the voltages u_1 and u_2 are given by:

$$\begin{aligned} &sin(x_1)x_3 - cos(x_1)x_4 = \rho cos(x_1), \\ &u_1 = Rx_3, \\ &u_2 = Rx_4. \end{aligned} \tag{3.18}$$

This analysis is consistent with what one sees in step motors in practice, where it is possible to maintain the motor stopped at one specific angle by applying the correct current value in each phase. In the case of a hybrid step motor with a chopper driver, this state means a high frequency PWM voltage signal controlling the steady state constant current.

4 STEP SYSTEM OPTIMAL OPERATION: SIMULATION RESULTS

This chapter presents and describes the Simulink© model used to perform both closed loop and open loop analysis together with a proposed framework for a generic performance analysis of step systems.

4.1 Driver and hybrid step motor *Simulink*© model

Given that the nature of the problem is moving the arm by a given distance within minimum time, simulations using the *power stepper motor* tool from *MatLab/Simulink*© were performed to analyse the system. For better understanding, the author will define one simulation as each time the *Simulink*© model is executed to simulate the arm moving from a defined initial angle θ_0 to a reference angle θ_{ref} at a given constant speed ω starting from rest.

To use the *power stepper motor* module from *MatLab/Simulink*©, the user must provide an input "*STEP*" signal with values 1 or 0 to determine whether the driver will energize the motor or not. As long as it receives a pulse of value one, the driver will make current flow through the windings according to its configuration. The input "*DIR*" receives a signal of value 1 or -1 and tells the driver which winding to energize first and the direction of the current in one of the windings. This will make the motor rotate counter-clockwise for $DIR = 1$, or clockwise for $DIR = -1$. Figure 22 shows de default *power stepper motor* diagram when opening the toolbox.

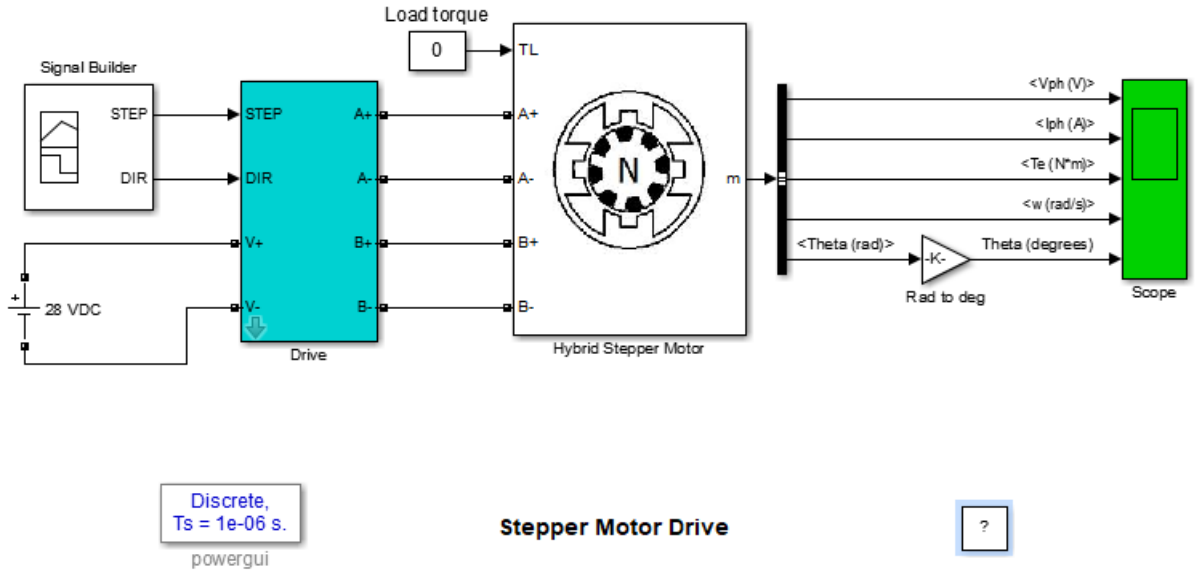

Figure 22: Default *power stepper motor* module diagram.

Source: *MatLab*©

4.1.1 The driver module

The driver module accepts a input DC voltage source input, which configures the power supply. It is detailed in Figures 23 and 24, respectively, for the default module and the modified module, used in the closed loop simulations. The highlighted square shows the part of the block that was modified. The driver needed modifications due to the fact that the default block is built for only one speed set up through a single simulation, whereas for the closed loop simulations described in section 4.3 there was the need to change the speed of the motor (e.g, the drivers pulse rate) in a single simulation.

The highlighted square in Figure 23 shows the part of the block that builds the excitation signal frequency (defined by the parameter "*pulse_rate*" of the driver block) and amplitude according to the desired speed and micro stepping rate (i.e, in this case 1600 PPR). This will be later multiplied by two lookup tables, one for each phase of the motor, and then weighted by the reference current to define the excitation sequence through time. This excitation signal will define for how long the reference current will stay in a certain level, obeying the desired micro stepping rate, so the current will behave as in Figure 10.

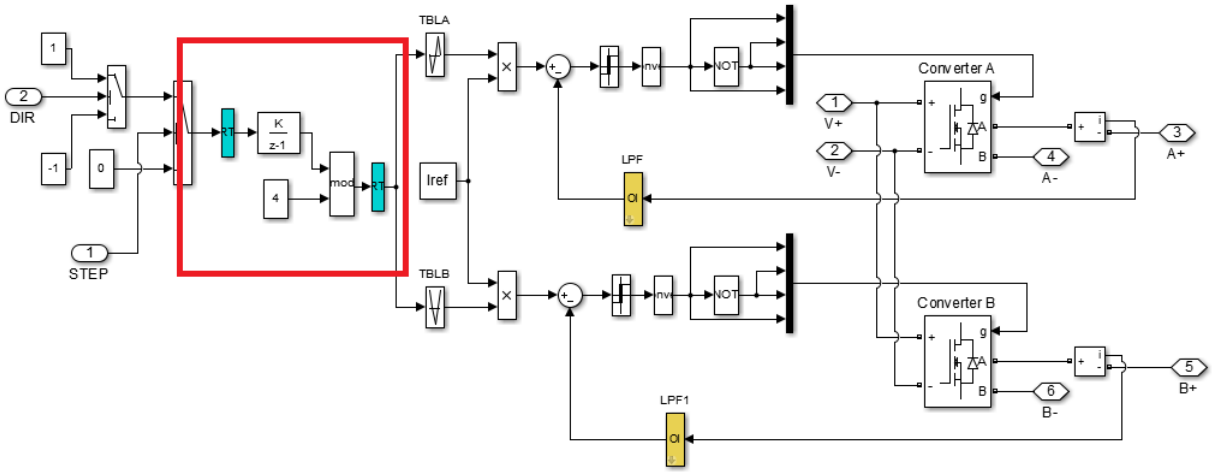

Figure 23: Default driver module diagram.

Source: *The author*

In Figure 24 the block that builds the excitation signal was modified by a custom function called "*driverSignalController*" in order to change its frequency during execution of a single simulation.

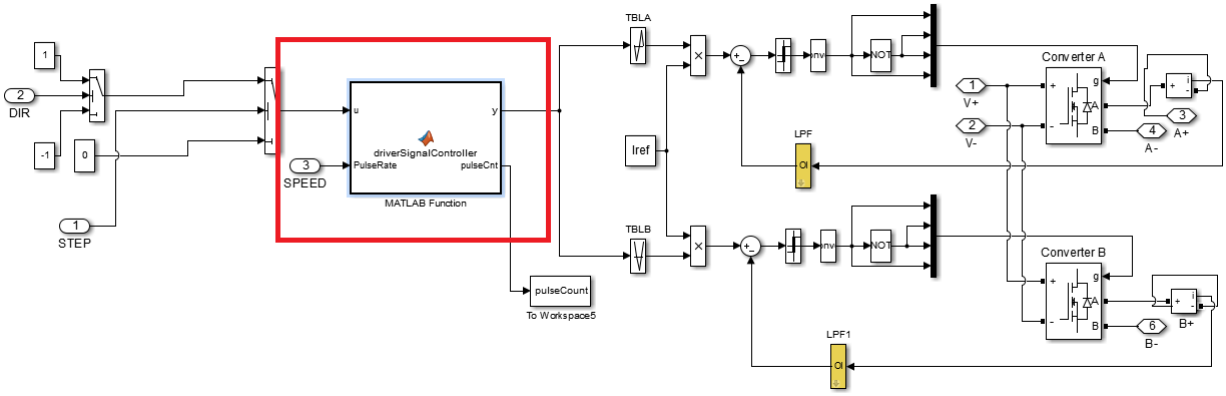

Figure 24: Modified driver module diagram.

Source: *The author*

At the left side of the highlighted square is the part of the block that controls the direction of movement and the enable signal (which defines when the motor is running or not). At the right side of the highlighted square is the current control circuit, composed by a MOSFET H-Bridge circuit (Converter A and Converter B in Figures 23 and 24), a current sensor to close the current control loop and to measure the current on the windings.

4.1.2 The motor module

The *power stepper motor* module implements the step motors equations described in section 2.2. Figure 25 shows the 3 main blocks of the model:: i) Windings, ii) Mechanical and iii) EMF (electromotive force).

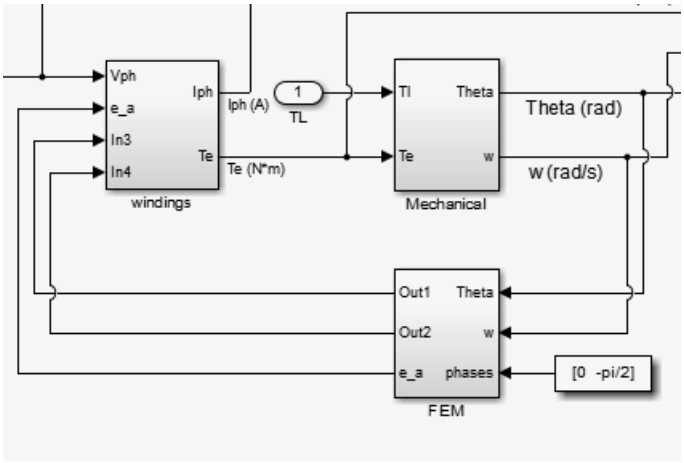

Figure 25: Diagram of the motor's module.

Source: *Simulink*©

Figure 26 details the block diagrams for the main blocks of the hybrid motor module presented in Figure 25:

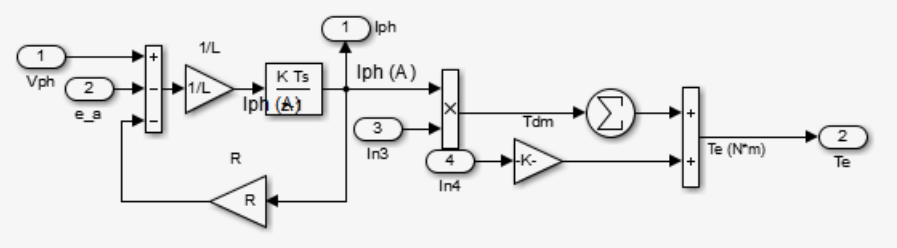

(a) Diagram of the motor's module windings block diagram.

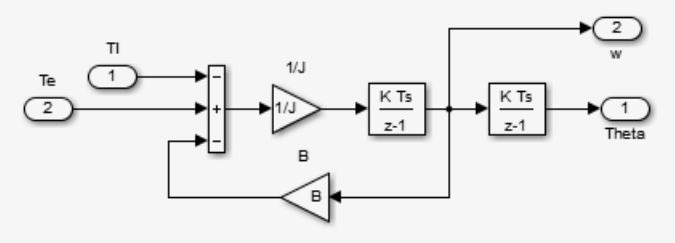

(b) Diagram of the motor's module mechanical block diagram.

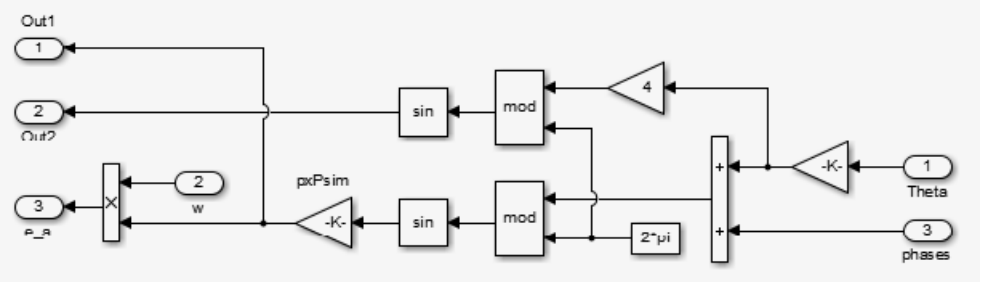

(c) Diagram of the motor's module EMF block diagram.

Figure 26: Details of the motor's module.

Source: *Simulink*©

One can note that these blocks implement the motor's Equations 2.1, 2.2 and 2.3 and 2.5, thus ensuring that analysing the simulations results corresponds to analysing the desired behaviour of the model presented in this work using a chopper driver (section 2.3).

4.2 Open loop scenario

The open loop simulations consist of defining an initial angle θ_0 and a target angle θ_{ref}, the pulse rate (i.e speed) and the maximum current. Then calculate the direction of the movement and the number of pulses, N_p, necessary to run the desired distance based on the selected micro stepping rate, which is a straightforward calculation, shown in Equation 4.1:

$$N_p = \frac{|\Delta\theta|}{PPR} \tag{4.1}$$

Finally, calculate the simulation time, t_{sim}, that is the duration time for the $Simulink^{©}$ model to run. It is important to calculate this time in order to change it from one simulation to another when performing several simulations for different speeds ω. The simulation time is given by Equation 4.2:

$$t_{sim} = \frac{N_p}{\omega} \tag{4.2}$$

The toolbox provides the feature for defining an initial speed. This feature was used for the open loop simulations, in order to simplify the system at first, so an acceleration ramp for departing the motor from rest was not implemented. It is done for the closed loop simulations scenario, instead the initial speed is define as ω for each selected value of ω.

Each simulation provides a visualization of the angle through time. Figure 27 shows an example of a simulation from $\theta_m = 0^o$ to $\theta_m = 30^o$ at a constant speed of $\omega = 1.1781 rad/s$. This simulation in particular has an execution time greater than necessary in theory, to acquire data for analysing the behaviour of the windings voltage and current at non-zero current and non-zero load condition (e.g., the motor is static holding the load at $\theta_m = 30^o$).

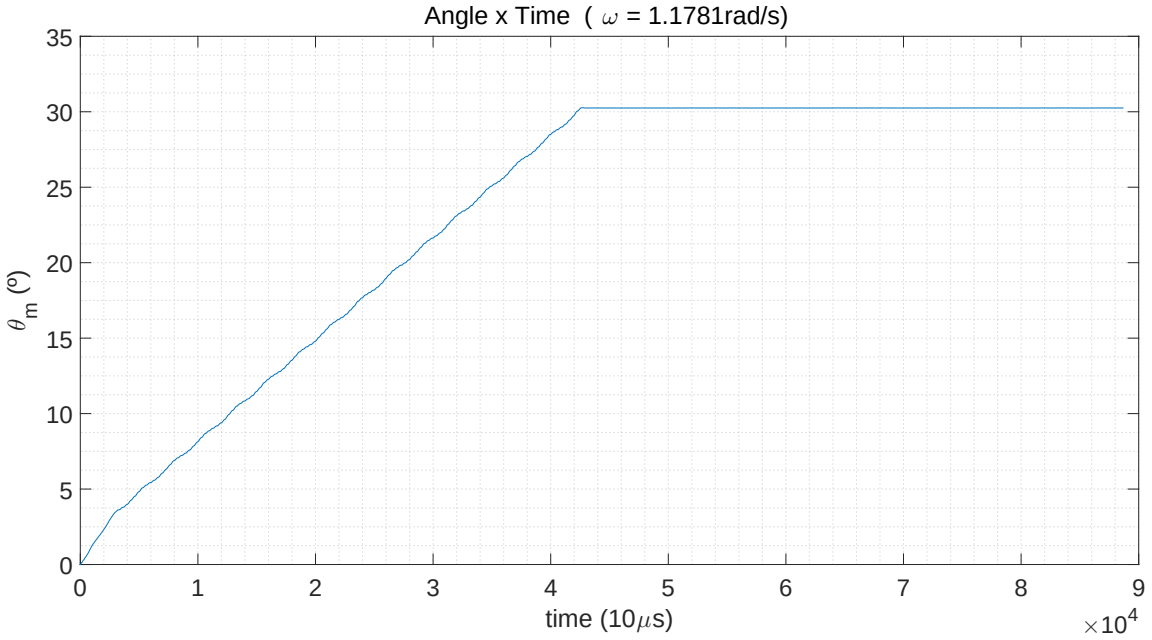

Figure 27: Angle output of one simulation from the *power stepper motor* module.

From this information, one can extract the value of the angle at the desired sample time. Sampling the angle at the specified pulse time and taking the difference between one sample to the next will result in the actual displacement between command pulses, $\delta\theta^*$ defined in Equation 4.3.

$$\delta\theta^*(n) = \theta_1(n) - \theta_1(n-1), \ \forall \ n = 1, 2, ...N_p. \tag{4.3}$$

In an ideal scenario, $\delta\theta^*$ is constant and equal to the programmed step angle $\delta\theta$. This however is not what happens in practice, where $\delta\theta^*$ presents small variations from $\delta\theta_{ref}$. In order to evaluate how far from $\delta\theta_{ref}$ (i.e, the configured micro stepping) the system is when performing a displacement of $\Delta\theta$, it is proposed to evaluate the mean of the actual displacement $\delta\theta^*$, define in Equation 4.4. This mean will give a single value at the end of the movement to evaluate if the system lost steps or not:

$$\mu_{\delta\theta} = \frac{1}{N_p} \sum_{n=1}^{N_p} \delta\theta^*(n). \tag{4.4}$$

Figure 28 shows the actual step angle taken by the motor through time. It is clear that there is an overshoot at the beginning due to inertia acceleration. However the motor tends to maintain an average step angle of $\mu_{\delta\theta} = 0.2254^o$.

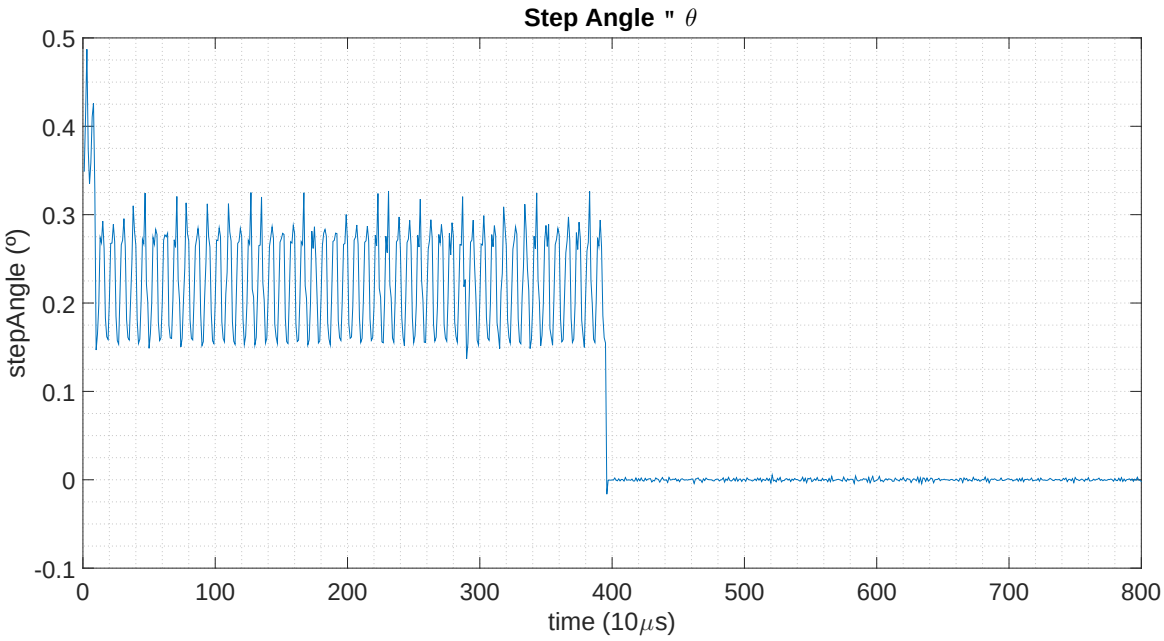

Figure 28: Step angle $\delta\theta$ output of one simulation from the *power stepper motor* module.

Source: *The author*

The mean of the difference $\mu_{\delta\theta}$, which represents the average distance travelled by the motor between command pulses, should be equal to the programmed $\delta\theta$ in an ideal scenario. When this mean starts to deviate from the reference value of $\delta\theta$ (i.e, the configured micro stepping rate, in this case $\delta\theta_{ref} = 0.2250^o$), it indicates that the motor is loosing steps. In other words, the rotor is not moving the distance that it is supposed to move between command pulses.

To evaluate the effectiveness of the motor in the system, several simulations were performed at different speeds ω (rad/s) resulting in curves like the one in a Figure 29. When $\omega \geqslant 2.0 rad/s$ the mean step angle $\mu_{\delta\theta}$ starts to deviates from the programmed step angle $\delta\theta = 0.2250^o$.

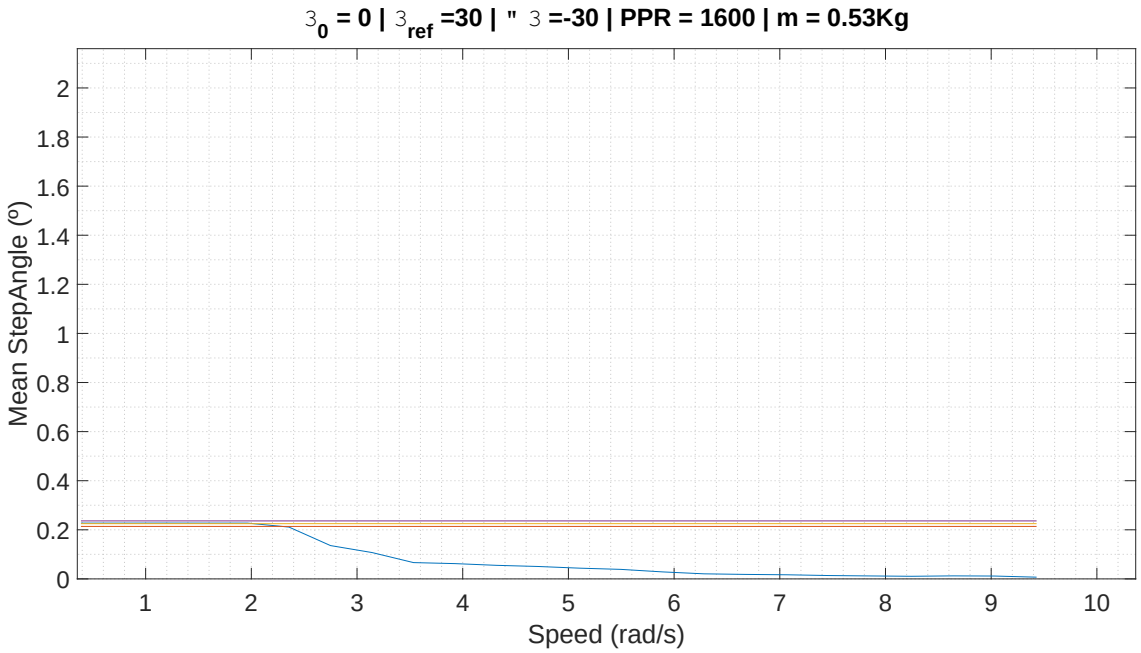

Figure 29: Average step angle $\mu_{\delta\theta}$ for several simulations at different speeds and the same reference angle θ_{ref}.

Source: *The author*

Analysing the speed range of $2.4 \leqslant \omega \leqslant 3.6$, approximately, gives the idea that the motor does loose steps, but does not necessarily enters a unstable state (i.e, when the system stops responding to command pulses), which is possible by closing the loop, so the system tends to become more robust and might be able to run at higher speeds. Specific studies should be done, but the completeness of this scenario suggests that an improvement is possible. This improvement is one of the main advantages of closing the loop of an usually open-looped system, allowing the use of a step motor in high speed and medium torque applications.

Plotting this curve for different target angles θ_{ref} results in a surface plot where one can evaluate the influence of the travelled distance on the unstable behaviour of the system. Figure 30 shows three different surfaces for three different initial angles θ_0 resulted from simulations with $m_g = 0.530\ kg$, $PPR = 1600$ and $I_{ref} = 6A$, which is the reference current for the driver. Several simulations for different stationary speeds, ω, are performed for each value of θ_{ref} in the interval [0°,90°].

The first and expected observation is that for high speeds ($\omega \geqslant 2\ rad/s$) the motor starts to loose steps and the mean stepped angle, μ_{δ_θ}, tends to zero. In another words, the motor tends to not move and starts to present an oscillatory behaviour. Another observation is that for $\theta_0 = 45°$ the mean stepped angled around θ_0 deviates a little from the reference even for low speeds.

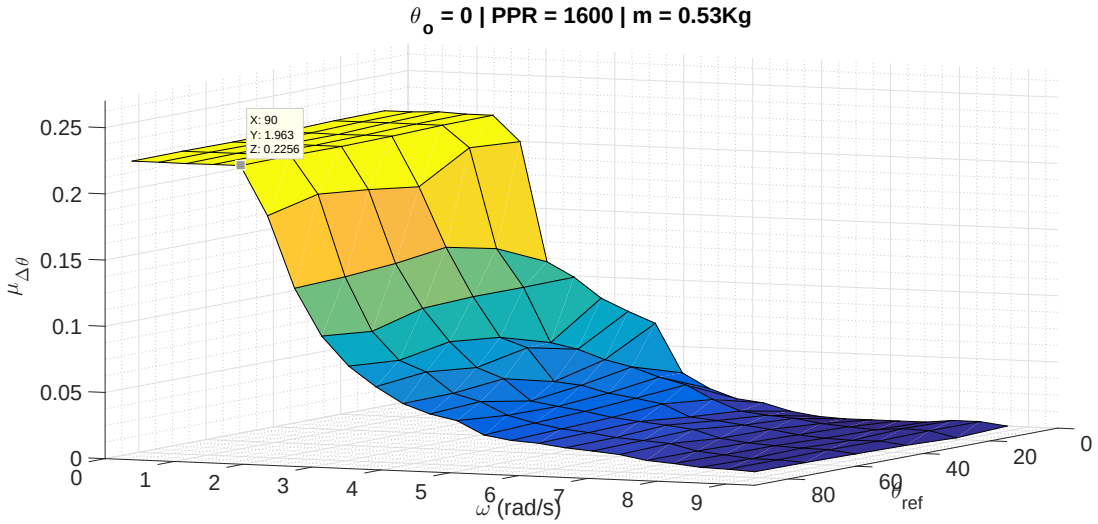

(a) $\theta_0 = 0^o$

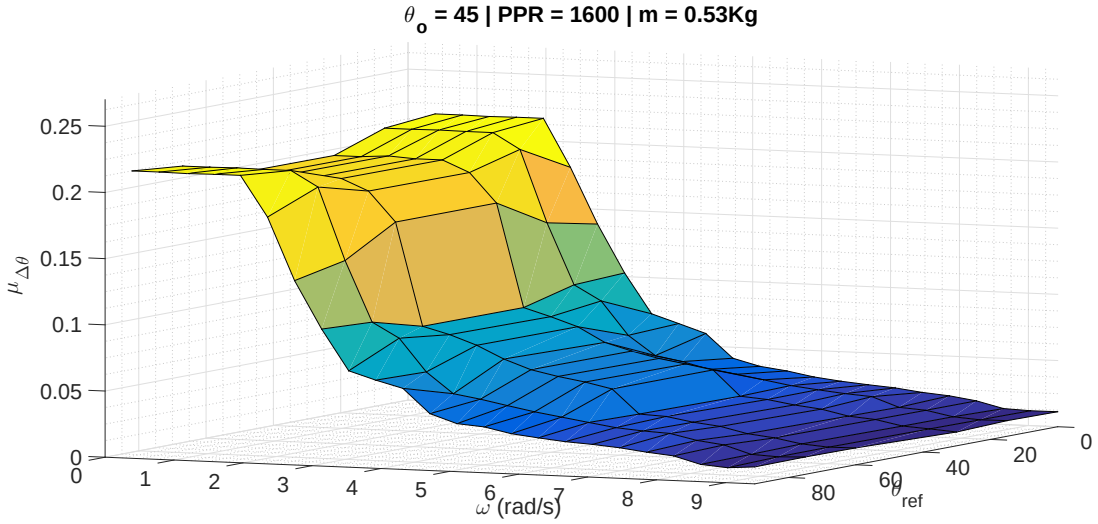

(b) $\theta_0 = 45^o$

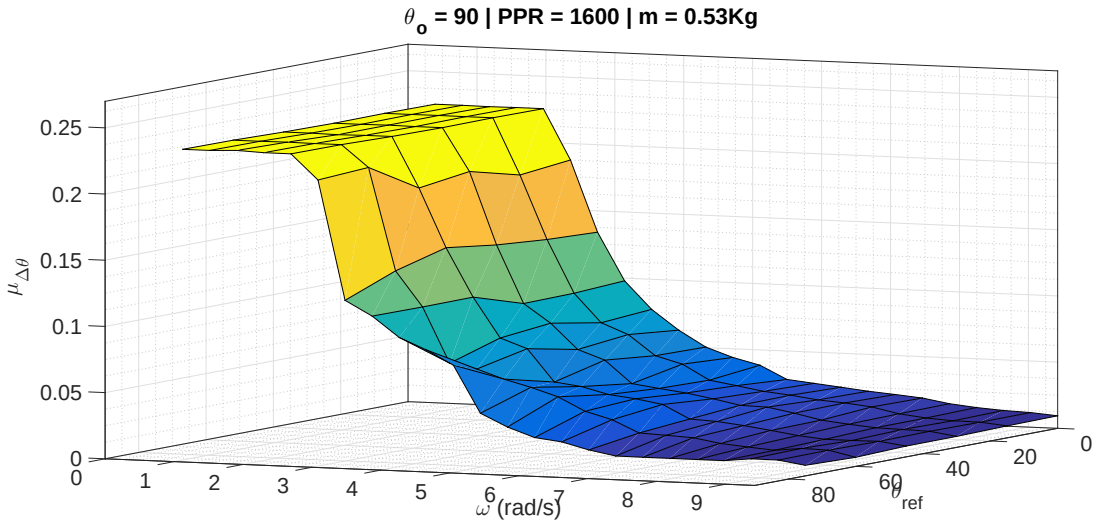

(c) $\theta_0 = 90^o$

Figure 30: Surfaces plot for three different initial angles.

Source: *The Author*

In open loop, in order to reach the desired angular position, one must operate the motor in the "plato" region of the surfaces in Figure 30a. The number of steps must be calculated in order to achieve the final position and applied to the driver.

4.3 Closed loop scenario

In closed loop form, which allows the operation in higher velocities (that is, when the surface is "falling" in Figure 30a, 30b and 30c), one can extend the possibilities of using the step motor in an application. Position feedback is used to track the position error and design a controller that sends pulses to the driver while the error does not reach a desired threshold, meaning that the number of pulses is no longer constant. This approach implies the need for a safety measure in case the step motor stalls, so the controller must monitor the trajectory evolution and detect a stall situation in order to stop the motor. For simplicity, this safety measure won't be covered in this work.

4.3.1 Description

The closed loop system operates using a controller that controls the position of the arm using the output angle error $\hat{e}(\theta_1)$ to adjust the speed in order to achieve the desired position at minimum time. Figure 31 shows the block diagram for the closed loop system. The idea to use position feedback to directly actuate in the speed of the motor comes from the fact that, for this case, when the arm approaches the desired position, the P controller automatically starts to decrease the speed of the motor, so no additional break system is necessary.

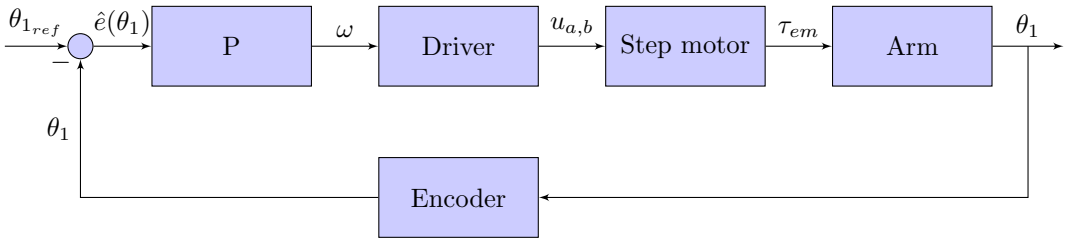

Figure 31: Block diagram of the closed loop system.

Source: *The author*

For the purpose of this work, which is to analyse the behaviour of the complete system, combining the actuator and motor models together, a simple proportional controller with gain of $P = 100$ was chosen to evaluate this case study and to formulate the framework

described in the next section. However, more advanced versions of this controller should be an object of study for further works. In practice, the step motor needs an acceleration ramp to depart from rest and cannot change speed drastically, in order to ensure a smooth movement and preserve the mechanics of the system. Therefore, the motor's acceleration and the controller's frequency of actuation were predefined to simplify the analysis. Figure 32 shows the modified *Simulink*© model.

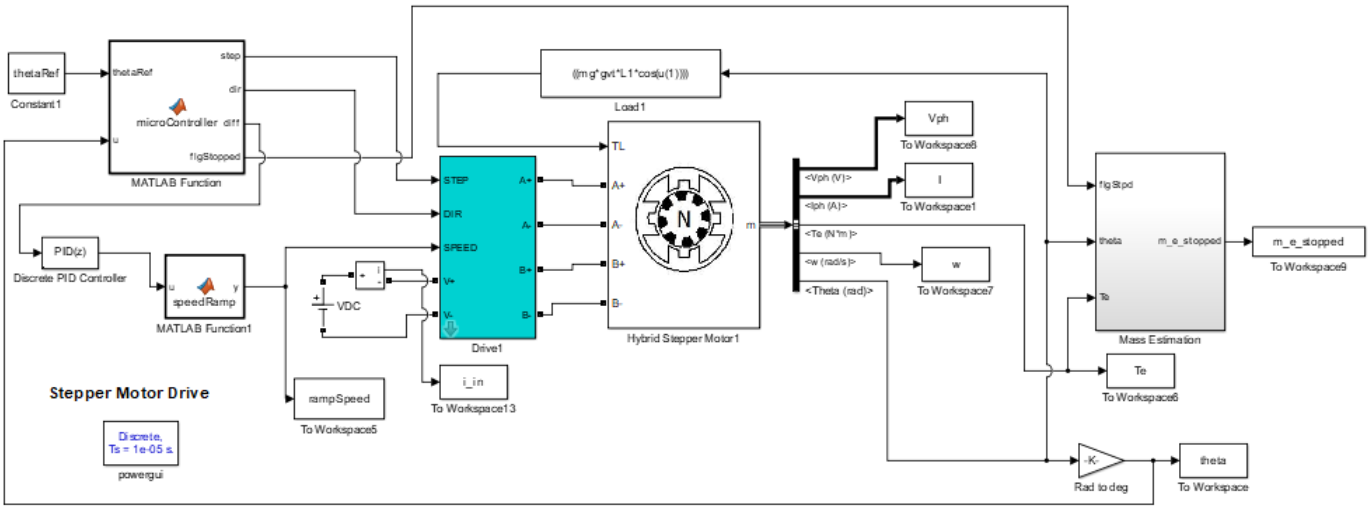

Figure 32: Modified *Simulink*© model.

Source: *The author*

The modified *Simulink*© model presents the following extra components:

- **microController:** A *Matlab*© function block that implements the micro controller functions that reads the encoder signal, calculates de error $\hat{e}(\theta_1)$ and sends it to the Discrete PID controller block. It also controls the STEP and DIR inputs of the driver and sets a flag when the motors stops, that is used by the mass estimation block.

- **speedRamp:** A *Matlab*© function block that implements the acceleration ramp when the motor starts from rest and sets the upper limit for the PID controller block.

- **Load 1:** This block implements the load torque τ_L equation as an input into the hybrid step motor block.

- **Mass Esimation:** This block implements the mass estimation, detailed in section 5.2.

Once the motor is accelerated, ideally, the controller should be free to achieve a maximum speed. This idea, however, is not straightforward when it comes to step motors, due to the *Speed X Torque* trade-off mentioned in chapter 2. As the speed goes high, the torque diminishes and the motor will no longer respond to the desired micro stepping configuration, therefore $\mu_{\delta\theta} \rightarrow 0$, which means that for every command pulse, at high speeds, the motor will only perform a fraction of the configured $\delta\theta$.

The controller needs a saturation value, ω_{max}, to ensure that the motor will not increase the speed indefinitely, leading to a loss of synchronism. In this scenario the saturation speed ω_{max} (i.e, the maximum speed of the system) is defined as the maximum speed the controller will allow the system to run, to travel the distance between any given initial angle $\theta_{1_{ini}}$ and the target position $\theta_{1_{ref}}$, defined as $\Delta\theta_1$. The time taken to go through $\Delta\theta_1$ is defined as $\Delta t_1 = t_1 - t_0$.

4.3.2 Examples

To illustrate this behaviour, we will show in the following the simulations of the angle $\theta_1(t)$, speed $\omega(t)$, current $I(t)$ and controller output $PPS_{ref}(t)$ for three different saturation speeds: $\omega_{max} \in [0.9817, 2.3561, 3.5343]$ and $\theta_{ref} = 135^o$. Figures 33, 34 and 35 show, respectively, simulation results for $\omega_{max} = 0.9817\ rad/s$, $\omega_{max} = 2.3561\ rad/s$ and $\omega_{max} = 3.5343\ rad/s$. It is possible to note that for $\omega_{max} = 2.3561$ the system starts to loose steps, but the time Δt_1 is smaller than for $\omega_{max} = 0.9817$. However for $\omega_{max} = 3.5343$, $\Delta t_1 \approx 1.9\ s$, which is higher than $\Delta t_1 \approx 1.175\ s$ for $\omega_{max} = 2.3562$, and one can note that the step loss is more significant and more notable at the angle profile.

Figure 36 shows the same results for the case where the P controller has no upper saturation limit. In another words, ω_{max} is not defined and the controller is free to increase the pulse frequency, PPS_{ref}, sent to the driver. For this situation, it is important to notice that the motor does not move forward after 0.8 s, keeping still at $\theta_1 = 25^o$, which is the main reason because the controller needs a saturation speed ω_{max}.

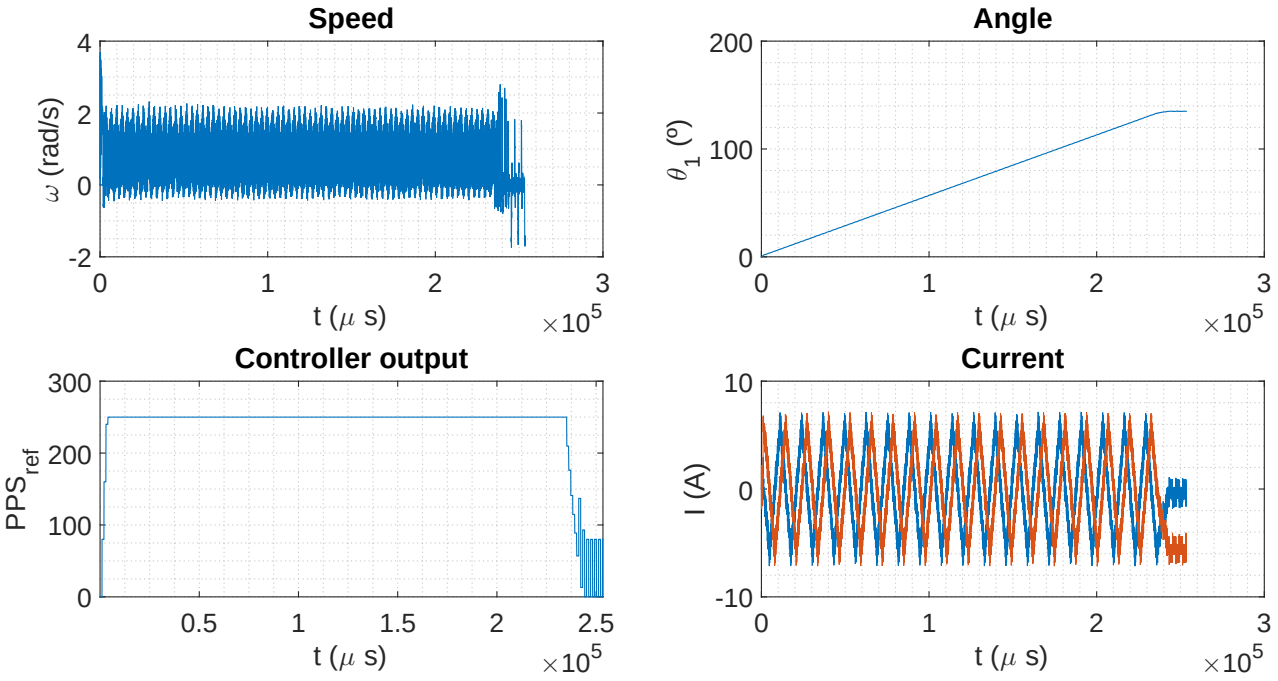

Figure 33: Simulation results for $\omega_{max} = 0.9817\ rad/s$

Source: *The author*

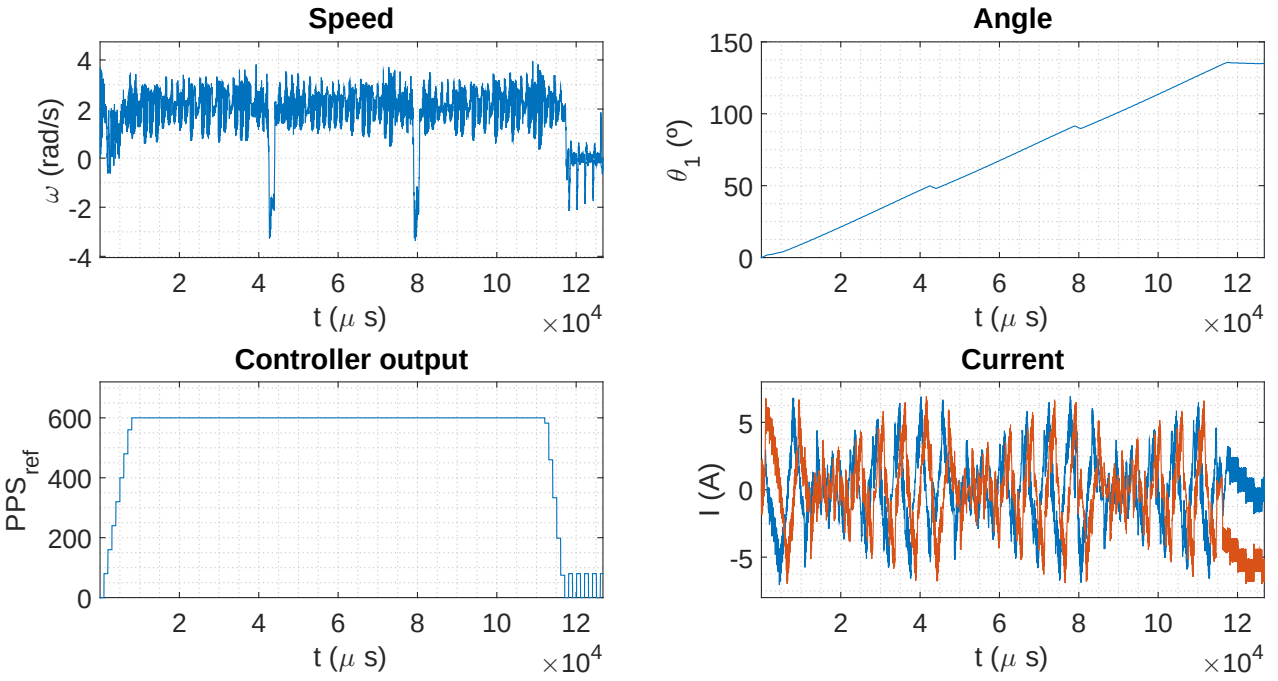

Figure 34: Simulation results for $\omega_{max} = 2.3562\ rad/s$

Source: *The author*

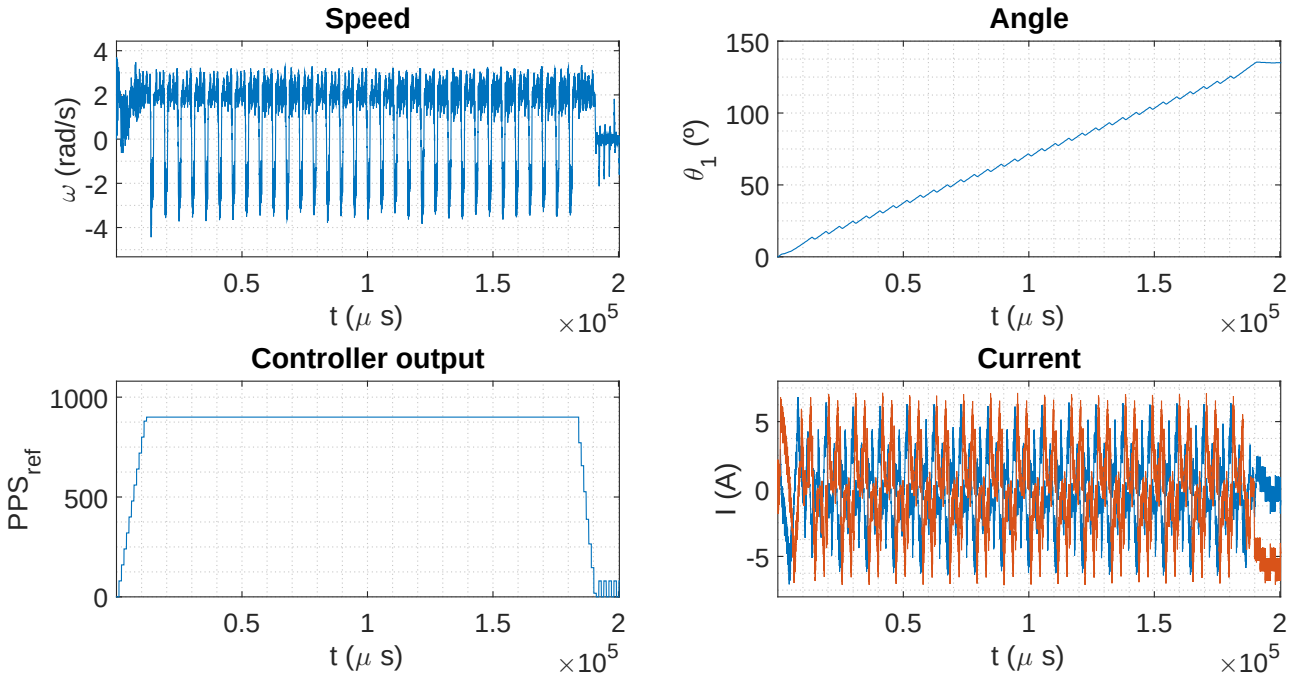

Figure 35: Simulation results for $\omega_{max} = 3.5343\ rad/s$

Source: *The author*

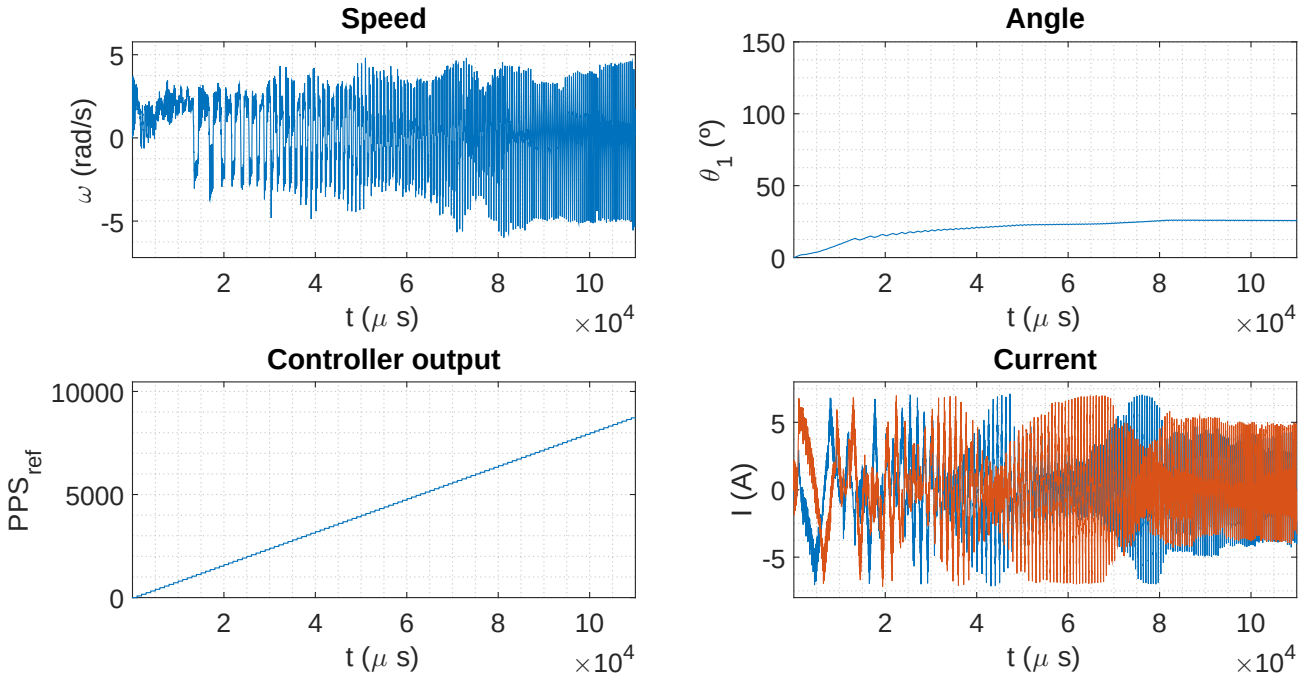

Figure 36: Simulation results when ω_{max} is not defined (the controller has no upper saturation)

Source: *The author*

4.3.3 Objective of the present application

The goal of the arm is to move the coconut in the smallest time possible, in another words, to find the maximum saturation speed ω_{max} that minimizes Δt_1 while maintaining the value of $\mu_{\delta\theta}$ as close as possible to the configured step angle (in this case is $\delta\theta = 0.2250\ ^{o}/p$), which leaves the question:

For a given load driven by a given step motor, what is the maximum speed in which that motor can drive the load, before the configured step angle $\delta\theta$ ***reaches a value from which the time*** Δt_1 ***starts to increase as speed increases, instead of decreasing?***

The idea to answer this question, is to define a framework to analyse the performance for a system driven by step motors, so the designer can have at the end of the process, enough data to decide which operation speed best suits its application.

4.3.4 Performance analysis framework

4.3.4.1 Parameters definition

The main idea is to define a set of parameters to be analysed, in order to decide the best operating zone for the given application. These parameters should be general enough to make sense for every application. They are detailed below:

- **Time** Δt_1**:** The overall time that the motor took to travel a given distance.
- **Mean Stepped** $\mu_{\delta\theta}$**:** The mean of the actual step travelled by the motor for each command pulse. This parameter indicates whether or not the motor is operating the desired micro stepping configurations. As speed increases and the motor begins to stall, the mean tends towards zero until the motor looses synchronism.
- **Energy** (E)**:** The overall energy consumption for a given distance $\Delta\theta$. This parameter is useful to analyse the control effort spent to move a load from a given position $\theta_{1_{ini}}$ to a desired position $\theta_{1_{final}}$.

  The energy analysis can be performed in four main components of the system: i) the input energy E_{in}; ii) the energy generated by the motor E_{em} and iii) the mechanical energy E_m and iv) the total energy of the load E_{tot}. They are described below:

  – **Input energy** E_{in}: Is the integral of the input power over time given by

Equation 4.5:

$$E_{in} = \int^{\Delta t_1} P_{in}\ dt = \int^{\Delta t_1} V_{dc} I_{in}\ dt, \tag{4.5}$$

where V_{dc} and I_{in} are, respectively, the voltage and the current of the input power supply.

– **Motor energy** E_{em}: Is the integral of the power delivered to the motor over time, given by Equation 4.6:

$$E_{em} = \int^{\Delta t_1} P_{em}\ dt = \int^{\Delta t_1} V_i I_i\ dt\ \forall\ i = 1, 2, \tag{4.6}$$

where V_i and I_i are, respectively, the voltage and current at the windings for each phase, $i = 1, 2$, of the motor.

– **Mechanical energy** E_m: Is the integral of the power at the output shaft over time given by Equation 4.7:

$$E_m = \int^{\Delta t_1} P_m\ dt = \int^{\Delta t_1} \tau_{em}\omega\ dt, \tag{4.7}$$

where τ_{em} is the torque delivered by the motor and ω is the output shaft's speed.

– **Stored energy** E_{stored}: Is the integral of the sum of the kinetic and potential energies, resulting from combining Equations 3.4 and 3.5, shown in Equation 4.8:

$$E_{stored} = K + U = \frac{1}{2} m_g \dot{\theta_1}^2(t) L_1^2 + m_g g L_1 sin(\theta_1(t)). \tag{4.8}$$

4.3.4.2 Parameters analysis

From the energy analysis, naturally follows an efficiency analysis, comparing how much energy is lost in a step motor driven application. The goal here is to separate the energy analysis, and to study the loss on both the driver system and on the mechanical system (i.e, the robotic arm). In order to do so, two different efficiency parameters were defined: i) electric efficiency Eff_e and ii) mechanical efficiency Eff_{em}. The electric efficiency, defined in Equation 4.9, represents how much energy is lost from the input power source to the motor, in another words, how much of the input energy is available for the motor to drive the load:

$$Eff_e = \frac{E_e}{E_{in}}. \tag{4.9}$$

The mechanical efficiency, defined in Equation 4.10, represents how much energy delivered by the motor is converted to the output shaft, in another words, it represents how good a step motor is in converting electrical energy to mechanical energy:

$$Eff_{em} = \frac{E_m}{E_{em}} \tag{4.10}$$

In order to analyse the efficiencies involved in the process and to best visualize the losses, the author proposes to compare the overall efficiency (electric and mechanical) with the first parameters defined in the framework, named time Δt_1 and mean stepped $\mu_{\delta\theta}$. Figures 37 and 38 show, respectively, Δt_1 and $\mu_{\delta\theta}$ on the left *y-axis* on a dashed line and, both Eff_e and Eff_{em} plotted together, in function of the maximum speed ω_{max}, on the right *y-axis*. The dotted line represents the mechanical efficiency Eff_{em} and the dot-dashed line represents the electrical efficiency Eff_e. The vertical solid line marks the speed in which the minimum time is achieved (considered all the values ω_{max} simulated), which is $\omega^*_{max} = 2.26\ rad/s$, and the *textbox* displays the parameter value as well as the efficiencies values for $\omega^*_{max} = 2.26\ rad/s$.

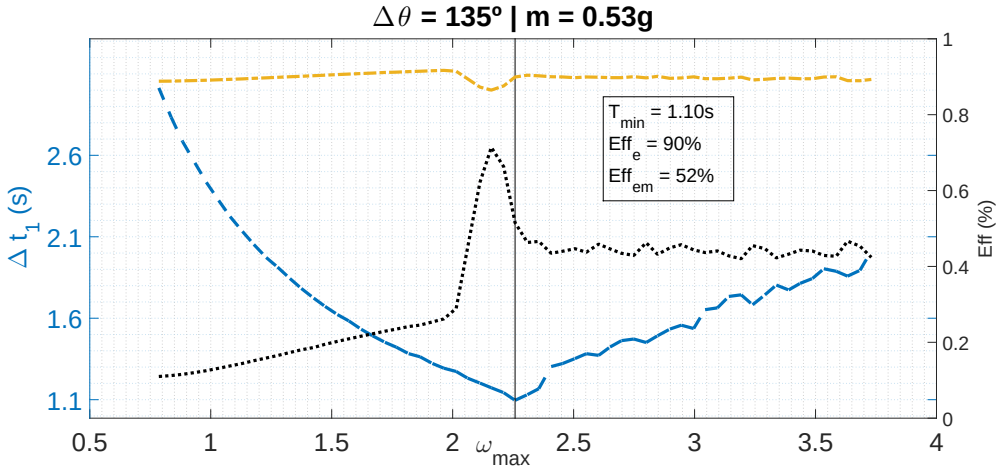

Figure 37: Efficiency analysis by time. The blue dashed (Δt_1) line should be read with the left y-axis whereas the yellow dot-dashed (Eff_e) and black dotted (Eff_{em}) lines should be read with the right y-axis (Eff)

Source: *The author*

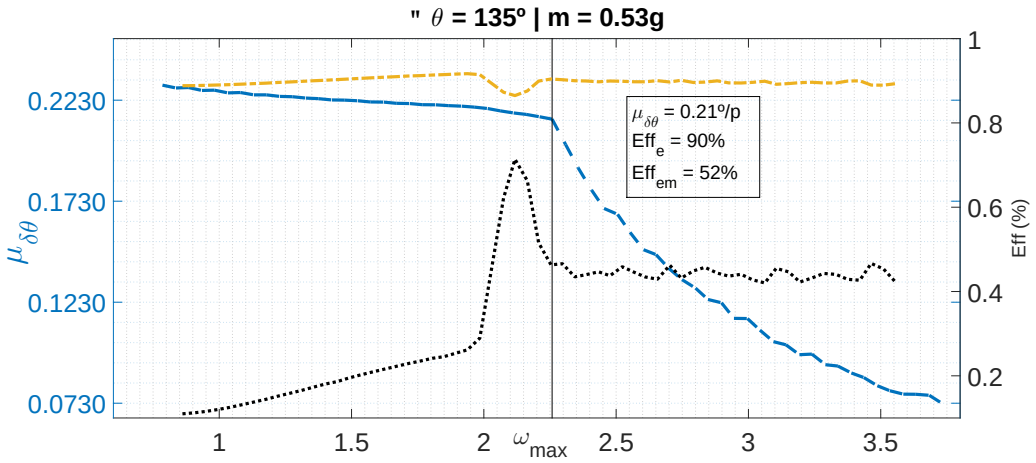

Figure 38: Efficiency analysis by mean stepped. The blue dashed (Δt_1) line should be read with the left y-axis whereas the yellow dot-dashed (Eff_e) and black dotted (Eff_{em}) lines should be read with the right y-axis (Eff)

Source: *The author*

First, note that both efficiencies increases as speed goes higher, Eff_e from approximately 0.85 to 0.9 and Eff_{em} from approximately 0.1 to 0.25. Then the Eff_e drops due to the fact that both input energy E_{in} and the motor energy E_{em} drop, thus leading to an increase in the mechanical efficiency Eff_{em}. Figure 38 shows that the point $\omega_{max} \approx 2.26\ rad/s$ is the point where the parameter $\mu_{\delta\theta}$ starts to drop exponentially, leading to the time increase seen in Figure 37. It is also the point where minimum time is achieved and the electrical and mechanical efficiencies are, respectively, $Eff_e = 90\%$ and $Eff_{em} = 52\%$. For $\omega_{max} \geqslant 2.26\ rad/s$ the time starts to increase and the mechanical efficiency stabilizes around 45%. This happens due to the fact the the torque of the motor drops drastically, so an increase in speed will not be converted in a better mechanical efficiency.

On the contrary, an increase in speed will result in higher friction loss. For the total energy, it is useful to analyse how much energy is lost when driving the load. Define the friction energy, E_{fric} as the difference between the mechanical energy and the stored energy, which is the energy needed to drive the load, as in Equation 4.11::

$$E_{fric} = E_m - E_{stored}. \tag{4.11}$$

Equation 4.11 shows that the higher the speed, which increases E_m, the higher will be the energy lost in the process. This loss depends only on the speed of the application, which will reflect on the mechanical system that will have to dissipate this energy. For the arm presented in this case study, this heat dissipation is not an issue. However it might be an

issue in other step motor driven systems.

Figure 39 shows the energies E_{em}, top line, and E_{stored}, bottom line and light shade, over time, for different values of speed. The dark shaded area represents the energy lost E_{fric}. The area of the dark shaded area is the mean of E_{fric}, defined in equation 4.12, which increases as ω_{max} increases (which is expected, since the higher the speed the higher the power dissipated).

$$\mu_{E_{fric}} = \frac{1}{S}\sum_{k=0}^{S} E_{fric}(kN), \tag{4.12}$$

where S is the number of samples

At the top of each graph it is displayed the value of ω_{max} together with the value of $\mu_{E_{fric}}$.

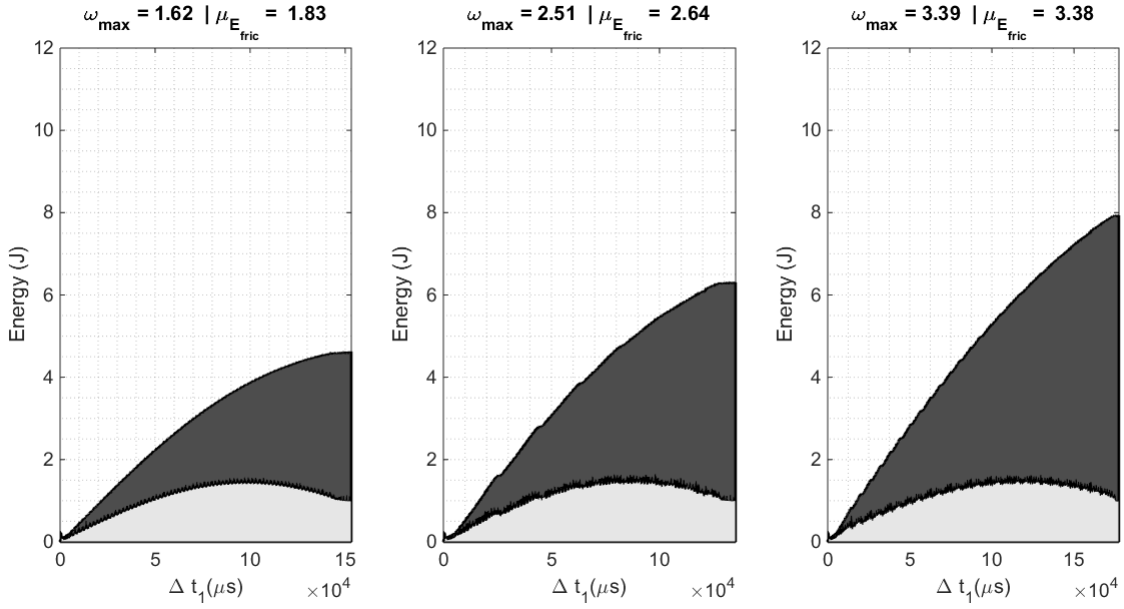

Figure 39: Energy analysis.

Source: *The author*

Figure 40 shows an energy flow diagram for a given $\Delta\theta$ travelled with a given ω_{max} as the speed saturation for a given mass m_g. This diagram represents most case scenarios (for different values of mass m_g and displacements $\Delta\theta$).

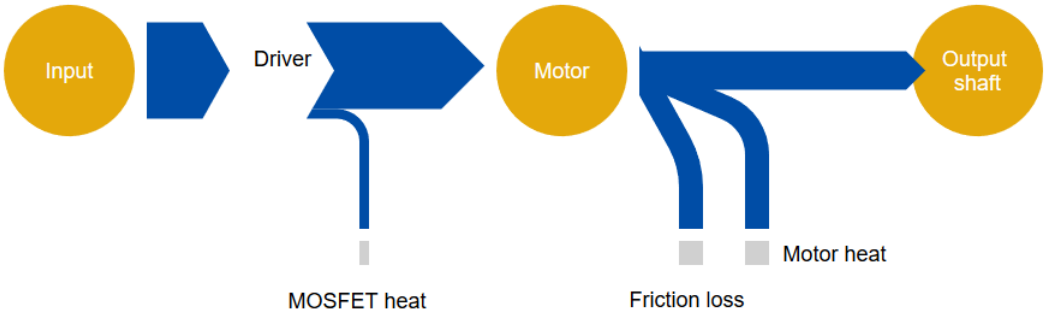

Figure 40: Energy flow diagram for an operation of the arm.

Source: *The author (created with www.sankeyflowshow.com)*

5 LOAD MASS ESTIMATION

This chapter presents the load mass estimation problem together with the proposed approach to solve it.

5.1 Mass estimation importance

Another important problem in the coconut paring system is the mass estimation. It was said that the paring process should save the maximum of coconut pulp as possible, and future additional systems could use the mass information in order to achieve minimum waste. A precise estimation of the coconut's mass can also be used to measure of the performance of the machine without adding an extra step prior to the coconut processing.

With the coconut properly weighed, measuring the machine's performance is achieved directly weighting the coconuts after the process, which is simpler and can be done on batches of several fruits at once. The machine's performance, ρ_m, can be defined as the total weight after the process by the weight before the process, as shown on Equation 5.1.

$$\rho_m = \frac{w_a}{w_b}. \tag{5.1}$$

where:

- w_b: Is the total weight before the processing.
- w_a: Is the total weight after the processing.

This overall performance, depends on several aspects of the operation, such as, the format and size of the fruits, as well as the speed of the process.

5.2 The proposed approach

Since the mass directly affects the load torque τ_L, as stated in Equation 3.7, the suggested approach for this scenario is to calculate the motor torque when the arm is stopped at a given final position θ_1. From Equation 3.10, it is possible to isolate the load torque and the motor torque. Analysing the second state-space equation when the motor is stopped, it is possible to derive a equation to estimate the mass, which is shown in Equation 5.2.

$$\begin{aligned}
\dot{x_2}(t) &= \frac{\psi_m[-sin(nx_1(t))x_3(t) + cos(nx_1(t))x_4(t)] + m_g g L_1 cos(x_1(t)) - Bx_2(t)}{J_{tot}}, \\
\cancelto{0}{\dot{x_2}(t)} &= \frac{\psi_m[-sin(nx_1(t))x_3(t) + cos(nx_1(t))x_4(t)] + m_g g L_1 cos(x_1(t)) - B\cancelto{0}{x_2(t)}}{J_{tot}}, \\
\psi_m[-sin(nx_1(t))x_3(t) + cos(nx_1(t))x_4(t)] &= m_g g L_1 cos(x_1(t)), \\
\\
m_g &= \frac{\psi_m[-sin(nx_1(t))x_3(t) + cos(nx_1(t))x_4(t)]}{g L_1 cos(x_1(t))}.
\end{aligned} \tag{5.2}$$

Equation 5.2 is an approximate equation due to the fact that the motor is operated by a chopper driver controlling the current at high frequencies, which leads to small variations in current and in the final angle. These variations can be however suppressed using a moving average filter to filter the high frequencies of the signal and extract a DC value. The proposed approach is to sample the current and arm angle signals at a sample period N, resulting in Equation 5.3.

$$m_g^*(kN) = \frac{\psi_m[-sin(nx_1^*(kN))x_3^*(n) + cos(nx_1^*(kN))x_4^*(kN)]}{g L_1 cos(x_1^*(kN))}, \forall k = 0, 1, 2 \ldots N-1. \tag{5.3}$$

where:

- $x_1^*(kN)$: sampled angle;
- $x_3^*(kN)$: sampled current from phase A;
- $x_4^*(kN)$: sampled current from phase B;
- $m_g^*(kN)$: sampled mass signal;

After sampled, the values are filtered in real time by a digital moving average window filter, shown in Equation 5.4:

$$m^*_{g_{avg}}(kN) = \frac{1}{W}\sum_{q=1}^{W} m^*_g(kN - q),\ \forall\ k \geqslant W, \tag{5.4}$$

where:

- W is the size of the window
- k is the current sample

This approach has the disadvantage of presenting a settling time for the moving average filter. However, due to the nature of the problem, the arm should remain stopped at a given position to wait for the paring table. This waiting time presented is sufficient, since the settling time of the filter turned out to be irrelevant in the simulations performed, resulting in that the beginning of the signal $m^*_{g_{avg}}(kN)$ can simply be ignored.

To calculate the mass estimation, the system performs a simple mean of a segment of the signal $m^*_{g_{avg}}(kN)$ from equation 5.4. The estimated mass $\hat{m_e}$ is then given by Equation 5.5:

$$\hat{m_e} = \frac{1}{S}\sum_{k=i}^{j} m^*_{g_{avg}}(kN), \forall k = i, i+1, i+2\ ...\ j, \tag{5.5}$$

where:

- i and j are the indices that define the interval chosen calculate $\hat{m_e}$, in another words, i and j define the time span that will be used to estimate the mass.
- $j \geqslant i$

The indices i and j are defined, respectively, by the initial delay t_i and the final measurement time t_f, chosen to calculate the mass, and by the sample period N. The time span of estimation is defined as $\Delta T_{calc} = t_f - t_i$. The number of samples inside ΔT_{calc} will, obviously, depend on the sample period N, since the number of samples, S, is defined as:

$$S = \frac{\Delta T_{calc}}{N} \tag{5.6}$$

Figure 41 shows an example of the signal $m^*_{g_{avg}}(kN)$ with $N = 1 \times 10^{-5}s$. The zero part of the signal corresponds to the movement of the arm. After the arm stops, the system starts to compute $m^*_{g_{avg}}(kN)$.

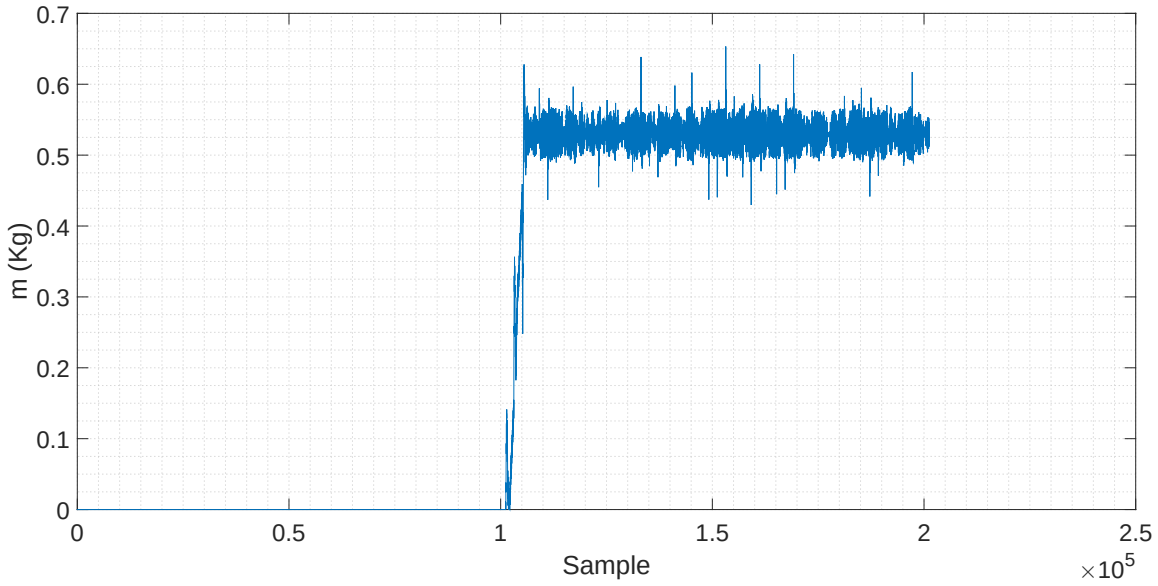

Figure 41: Mass signal $m^*_{g_{avg}}(kN)$ sampled at $10\mu s$.

Source: *The author*

Figure 42 shows the signal $m^*_{g_{avg}}(kN)$ sampled at $10\mu s$ marked with two dashed vertical lines at $t_i = 200ms$ and $t_f = 500ms$, resulting in a $\Delta T_{calc} = 300ms$. All these times are with respect to the start point of sampling (which is when the arm stops).

The value of $\Delta T_{calc} = 300ms$ was proven to be a good choice to calculate the estimated mass, $\hat{m}_e$. Figures 43 and 44 show the signal $m^*_{g_{avg}}(kN)$ for three different values of mass $m_g = 0.53, 0.64, 0.75kg$, respectively, for $N = 10\mu s$ and $N = 10ms$.

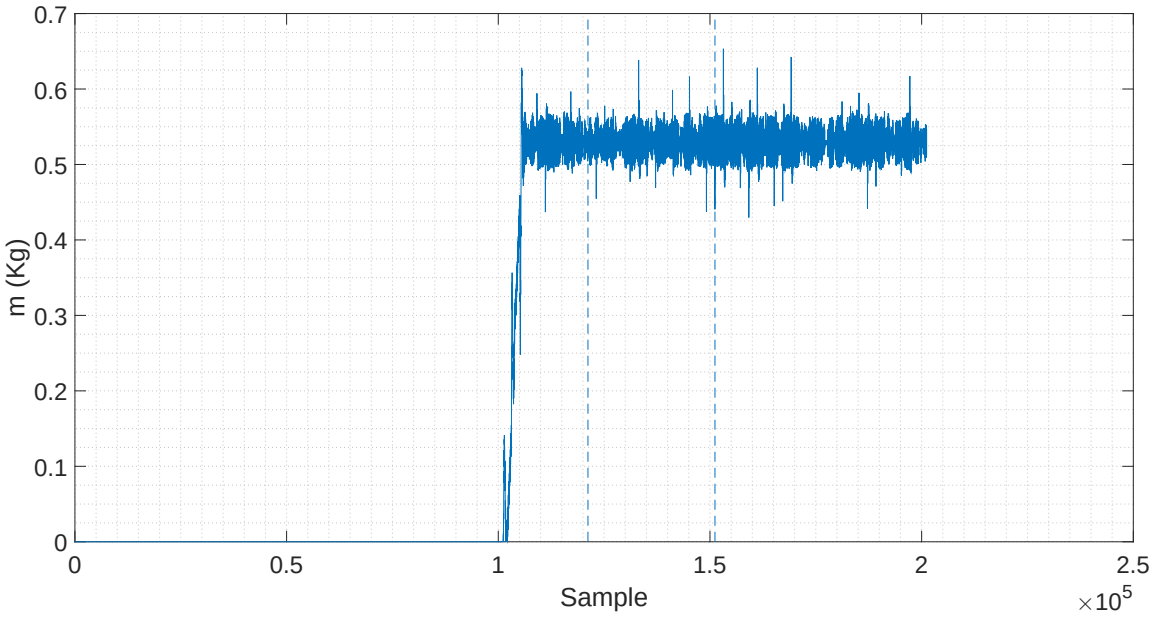

Figure 42: Mass signal $m^*_{g_{avg}}(kN)$ sampled at $10ms$.

Source: *The author*

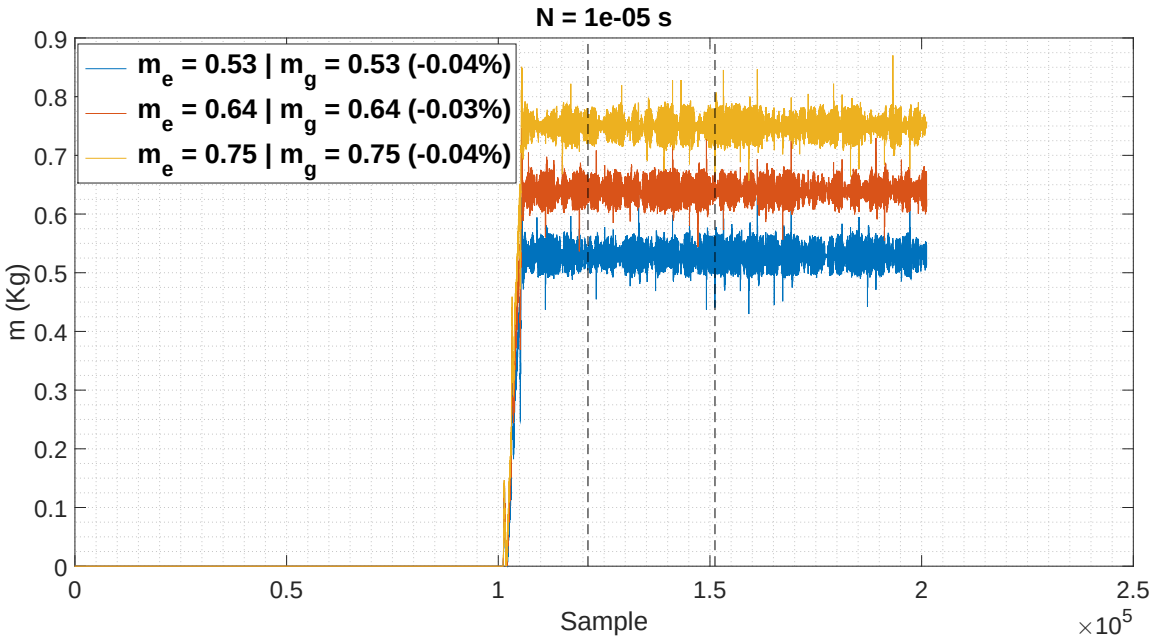

Figure 43: Mass signal $m^*_{g_{avg}}(kN)$ sampled at $10\mu s$ for 3 different values of m_g.

Source: *The author*

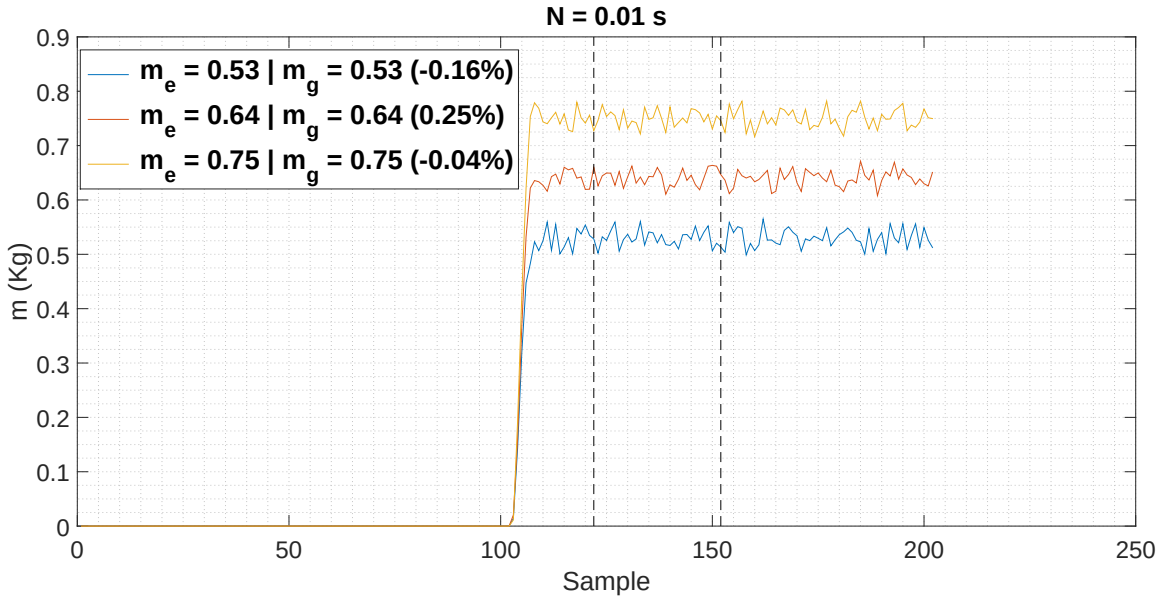

Figure 44: Mass signal $m^*_{g_{avg}}(kN)$ sampled at $10ms$ for 3 different values of m_g.

Source: *The author*

Table 1 summarizes the performance for each sample period, for the three values of mass simulated. The value of $\hat{m}_e$ is rounded up to 2 digits, resulting in a very precise estimation. The error value between the parenthesis represent the estimation error without rounding the estimation mass $\hat{m}_e$ value. Note that even though there is a difference in the estimation error between $N = 10\mu s$ and $N = 10ms$, the overall estimation is not affected.

This suggests that this method is a very good candidate to be tested in practice and is robust enough to be used in large sample periods (low frequencies). The lower the sample frequency, the fewer the number of samples to be computed and the faster the calculations can be performed. This is an important factor to consider when working with micro controllers.

m_g / N	0.53 kg	0.64 kg	0.75 kg
$10\mu s$	0.53 (-0.04%)	0.64 (-0.03%)	0.75 (-0.04%)
$10ms$	0.53 (-0.16%)	0.64 (0.25%)	0.75 (-0.04%)

Table 1: Mass estimation results.

6 CONCLUSIONS AND FUTURE WORK

This chapter concludes the work by summarizing its main contributions and identifying possible improvements that can be done in future works.

A brief review of the main aspects of a step motor was performed and its non linear mathematical model was presented, as well as combined with a dynamic load model derived from a 1 DOF robotic arm used to move a coconut from a buffer plate to the paring table. That is the motivating problem for this work.

This combined model was used to simulate and to study the behaviour of a complete robotic step system, simulated together with a step driver, thus making the simulations as close as possible to a practical operation. The model was adapted to work in closed-loop, which means that some modifications in the built-in $Matlab^{©}$ driver model were implemented. This approach allowed a more complete study of an application where the step motor operates on its limits in terms of speed. The first two main objective of this work were achieved by the study of the whole step system. The first one was to define a structured method for selecting a step motor for an application, presented in section 2.5.3. The second one was to formulate a framework to analyse the performance of a step system according to a set of useful generic parameters: i) time, ii) mean step and iii) energy consumption, presented in section 4.3.4. Figures 37 and 38 show the first two parameters as function of the max speed of the system, ω_{max}, and can be used as a visual tool to determine the best operating speed. These figures can also be used to validate that for ω_{max} greater than the optimal value, the mechanical performance of a step motor is around 45% for this scenario.

Considering that the complete driver system was simulated, it is enough to say that the proposed mass estimation approach could be tested in practice to evaluate its performance on the actual machine. Also, the time interval to achieve precision in the mass estimation was short and simple enough to be implemented in real time and with low computational burden. The load mass estimation was achieved with high confidence in

terms of estimation error, as presented in Table 1, through the analysis of the systems equation when the arm is stopped at a given position while being excited. Figures 43 and 44 show that the signal obtained by the chosen method is a well behaved signal and can be used for further practical studies of the problem.

A point of interest is the controller used to set the speed of the motor. Initially a simple proportional controller was chosen. However, it was noticed in the simulations that better performance can be achieved when using other controllers, like a PD controller or a artificial intelligence controller, using fuzzy logic, for example. In (JEONG; LEE; CHUNG, 2020) the authors present several advanced control methods for permanent magnet step motors, that can be used as a start point to investigate possible control schemes for future works.

REFERENCES

KHAN, T. A.; TAJ, T. A.; IJAZ, I. Hybrid stepper motor and its controlling techniques a survey. *Proceedings of the 2014 IEEE North West Russia Young Researchers in Electrical and Electronic Engineering Conference, ElConRusNW 2014*, p. 79–83, 2014.

HUGHES, A.; DRURY, B. *Electric Motors and Drives: Fundamentals, Types and Applications*. [S.l.]: Elsevier Science, 2013. ISBN 9780080993683.

HENKE, B. et al. *Modeling of hybrid stepper motors for closed loop operation*. IFAC, 2013. v. 46. 177–183 p. ISSN 14746670. ISBN 9783902823311. Disponível em: ⟨http://dx.doi.org/10.3182/20130410-3-CN-2034.00042⟩.

MORAR, A. The Modelling and Simulation of Bipolar Hybrid Stepping Motor by Matlab/Simulink. *Procedia Technology*, v. 19, p. 576–583, 2015. ISSN 22120173.

ACARNLEY, P. P.; WATSON, J. F. Review of position-sensorless operation of brushless permanent-magnet machines. *IEEE Transactions on Industrial Electronics*, v. 53, n. 2, p. 352–362, 2006. ISSN 02780046.

DRAAMMELAERE, S. et al. Robust sensorless load angle control for stepping motors. p. 1603–1608, 2015.

LIN, C.; CHEN, P.; CAO, Q. Research on torque-variable control method for stepping motors in service robot arm. *Proceedings of IEEE Workshop on Advanced Robotics and its Social Impacts, ARSO*, v. 2016-November, p. 85–90, 2016. ISSN 21627576.

CHUDASAMA, T.; BARIA. Speed and Torque Control of Stepper Motor using Voltage and Current Control. *International Journal of Research in Modern Engineering and Emerging Technology*, v. 1, n. 3, p. 10–14, 2013.

users.ece.utexas.edu. *Stepper motor and driver selection. [ONLINE] Available at:* . 2000. http://users.ece.utexas.edu/ valvano/Datasheets/StepperSelection.pdf. [Accessed 25 February 2018].

ROBERT, B.; ALIN, C.; GOELDEL, C. Aperiodic and chaotic dynamics in hybrid step motor - New experimental results. *IEEE International Symposium on Industrial Electronics*, v. 3, n. May, p. 2136–2141, 2001.

CORRON, N. et al. Eletric step motor non linear dynamics and estimation of the embedding dimension. 2001.

PERA, M.-C.; ROBERT, B.; GOELDEL, C. Nonlinear dynamics in electromechanical systems-application to a hybrid stepping motor. v. 7, n. 1, p. 31–42, 2000.

MILADI, Y.; FEKI, M.; DERBEL, N. Using unconventional methods to control the chaotic behavior of switched time systems: Application to a stepper motor. v. 6, n. 4, p. 81–89, 2013.

LYSHEVSKI, S. E. Microstepping and high-performance control of permanent-magnet stepper motors. *Energy Conversion and Management*, Elsevier Ltd, v. 85, p. 245–253, 2014. ISSN 01968904. Disponível em: ⟨http://dx.doi.org/10.1016/j.enconman.2014.05.078⟩.

Li, P.; Lu, H.; Shen, J. Analysis method of dynamic torque-frequency characteristic of hybrid stepping motors. In: *2017 Twelfth International Conference on Ecological Vehicles and Renewable Energies (EVER)*. [S.l.: s.n.], 2017. p. 1–6.

Dorin-Mirel, S.; Ion, M.; Mihai, O. The analysis of different frequency for a stepper motor open loop operation. In: *2016 8th International Conference on Electronics, Computers and Artificial Intelligence (ECAI)*. [S.l.: s.n.], 2016. p. 1–7.

SOUZA, D.; COLóN, D. Step Motor Selection and Control: An Industrial Case Study. *Congresso Brasileiro de Automática CBA2018*, 2018. ISSN 25258311.

MELKEBEEK, J. *Electrical Machines and Drives: Fundamentals and Advanced Modelling*. Springer International Publishing, 2018. (Power Systems). ISBN 9783319727301. Disponível em: ⟨https://books.google.com.br/books?id=G-xHDwAAQBAJ⟩.

Dejan Nedelkovski. *How a Stepper Motor Works. [ONLINE] Available at:* . https://howtomechatronics.com/how-it-works/electrical-engineering/stepper-motor/. [Accessed 12 March 2018].

ACARNLEY, P. *Stepping Motors: a guide to theory and practice*. [S.l.: s.n.], 2002. ISSN 00135127. ISBN 9780852964170.

MORAR, A. Stepper Motor Model for Dynamic Simulation. v. 44, n. 2, p. 117–122, 2003.

Mathworks©. Stepper motor and driver selection. [ONLINE] Available at: . 2007. https://www.mathworks.com/help/physmod/sps/powersys/ref/steppermotor.html. [Accessed 30 June 2020].

George. *Unipolar Stepper Motor vs Bipolar Stepper Motors. [ONLINE] Available at:* . 2012. https://www.circuitspecialists.com/blog/unipolar-stepper-motor-vs-bipolar-stepper-motors/. [Accessed 12 March 2018].

Derammelaere, S. et al. Torque ripples in stepping motor driven systems. *2015 17th European Conference on Power Electronics and Applications (EPE'15 ECCE-Europe)*, p. 1–6, 2015.

Geckodrive Motor Controls (GMC). *Step motor basics guide*. 2010. 1-17 p.

SPONG, M.; HUTCHINSON, S.; VIDYASAGAR, M. *Robot Modeling and Control*. [S.l.]: Wiley, 2005. ISBN 9780471649908.

JEONG, Y. W.; LEE, Y.; CHUNG, C. A survey of advanced control methods for permanent magnet stepper motors. In: . [S.l.: s.n.], 2020. p. 331–342.